1960

# Web buckling tests on welded plate girders, Part 3: Tests on plate girders subjected to shear, WRC Bulletin, 64, (September 1960), Reprint No. 165 (60-5)

K. Basler

J. A. Mueller

B. Thurlimann

B. T. Yen

3 Copies
No. 1

Welded Plate Girders, Report No. 251-13

Submitted to the
Welded Plate Girder Project Committee
for approval as a publication

# WEB BUCKLING TESTS ON WELDED PLATE GIRDERS

## Part 3: Tests on Plate Girders Subjected to Shear

by

Basler, K., Yen, B. T., Mueller, J. A., and Thürlimann, B.

Fritz Engineering Laboratory
Lehigh University
Bethlehem, Pennsylvania
May 1960

## FOREWORD

This paper is the third part of a report on plate girder tests conducted at Lehigh University. Reference must be made to the first part, Report No. 251-11, for the scheme of publication, the properties of the girders, the nomenclature, and the list of references.

## 3.1 Introduction

It has been pointed out that the postbuckling strength of plate girders subjected to bending is essentially provided by the compression flange. For girders subjected primarily to shear, the flange plates cannot increase the shear resistance to any degree and, therefore, the above conclusion cannot be made. Still, a rearrangement of stresses favorable for the web is possible which might utilize an element other than the web. Most likely, the element of paramount importance in the shear case is the transverse stiffener upon which a tension field might be supported.

The advancement of tension field action as an explanation for the postbuckling strength of plate girders is not a new idea. It originates from the design of lattice trusses which preceded the use of plate girders. Wagner, Ref. 258, was the first to mathematically formulate this concept for use in aircraft design. In civil engineering, however, this concept has seldom been applied for several reasons. One of these reasons is that in welded plate girders the flanges exhibit little rigidity in the vertical direction. Thus, one is reluctant to consider them as continuous beams supported by transverse stiffeners and

acting as the anchors of a tension field. The tests recently conducted by Massonnet on large size welded plate girders, Ref. 162, also seemed to discourage the idea of a tension field action.

Thus, the objective of this experimental investigation is to prove or disprove the occurance of a tension field action in welded plate girders as used in the Civil Engineering profession.

## 3.2 Design of Girders and Test Setup

The shear tests were conducted on a pair of girders which initially differed in the transverse stiffener spacing only. Similar to the bending girders, these shear girders were also composed of a test section, in which failure was expected to occur, and two end sections. With the setup illustrated in Fig. 1.2 of Sec. 1.1, (also Fig. 3.13), the test section was free from stress concentrations due to load introduction and contained as "pure a shear" as possible. This setup is shown in detail in Fig. 3.1, where the ordered dimensions of the girders are also given. With a web thickness of three-sixteenths of an inch, and the same web depth as in the bending girders, namely fifty inches, the girders had a web slenderness ratio of about 257. These girders, as well as the other girders in the

investigation, had some design details which differed from those generally followed. Although they are the subject of separate papers, some of these details are discussed here.

The Transverse Stiffeners were of two types, intermediate and bearing. All intermediate stiffeners were plates 4" x 1/4" welded continuously to both sides of the web and to the compression flange. The bearing stiffeners, used at loading and reaction points, consisted of T-sections cut from 12WF50 shapes and welded to the web such that the distance between their extreme fibers was eleven inches. Both types of stiffeners were made from regular A7 steel with a yield level, as measured by the mill, of around 43 ksi. All transverse stiffeners, whether bearing or intermediate, were cut one inch short of the tension flange in order to study the influence of this detail on the overall strength of the girder. It is interesting to note that not even in the shear girders did this short cutting of stiffeners have any detrimental effect. The results of the study on this single detail are presented and analyzed in Ref. 8, and therefore, are not treated any further here.

The cover plates were fillet-welded to the flanges of the plate girders. Plate dimensions are listed in Table 1.2

of Sec. 1.2. The weld sizes were determined by the assumption that the combined action of cover plate and flange is developed within a distance of about the width of the cover plate; beyond this distance, the weld size required by the conventional "VQ/It" method was used. Without much additional effort, the strains in the cover plates were recorded. The results of these readings, together with the results from gages mounted on a loading stiffener of G6, are compiled in a separate report, Ref. 273, and are interpreted in connection with Ref.269, and Ref. 270.

The Weld Sizes between the web and flanges were designed for the thinner of the two plates joined, in this case the web. As a rule, the sum of the throat dimensions of the two opposite fillet welds was chosen to be equal to the thickness of the web. Listed in Table 3.1 are the weld sizes at the intersection of web and flange for all girders. Except when accompanied by an asterisk which denotes hand welding, all welding was done with a submerged arc. Great care was exercised not to exceed the listed weld sizes. Since the ASTM manual requires that welds along a three-quarter inch flange must be at least one-quarter of an inch, the resulting welds were quite undersized in some of the girders' test sections as compared with the specifications. However, in no case did

the welds fracture prior to ultimate load. Even when greatly strained after the ultimate load to obtain an unloading curve, few fractures occurred. In one case web crippling reached such a magnitude during this unloading range that a crack in the web plate several inches long could be observed adjacent and parallel to the fillet weld. Certainly, since this happened in the unloading range, it has no bearing on the ultimate load. If any conclusion can be drawn, it is that a larger weld size would only have increased the residual stresses, causing the metal to become more brittle and making the "burning" effect more pronounced. The fillet weld should only be large enough to transmit the shear from the web to the flange.

Again, the establishing of such a welding detail was not the objective of the investigation. However, since the welds were smaller than required by specification and still had no detrimental effect on the carrying capacity of the girders, the tests on the thirteen girders bear mute testimony to the safety of present welding requirements.

## 3.3 Ultimate Loads and Web Deflections

The testing history of each girder is presented in a load-deflection curve. The cantilever end deflection

is chosen as the most significant deflection data since it reflects the effects of almost every girder element. The deflection at mid-span theoretically should be zero throughout the elastic range of the test. This is obvious in the first curve of Fig. 3.2 which shows the observed deflection line of girder G7 at load No. 5, 108 kips. By subtracting from the observed deflections those due to support movements, the true deflections, $V_e$, are obtained and used for the load-deflection curves. The second curve in the figure, for load No. 22 (zero kips), shows clearly the distortion of the girder shape after ultimate load and indicates that the mid-span deflection at this stage differs greatly from zero.

The correlation between the load magnitude P, as provided by each of the two jacks, and the cantilever end deflection $V_e$ is given in the so called load-deflection curves, Figs. 3.3 and 3.4. For the sake of convenience a second ordinate is added which lists the corresponding maximum shear stress as computed from the "VQ/It" formula. Yielding due to shear at the neutral axis of the girder's test section would be reached at a load indicated as $P_y$, while full plastification of the web due to shear would occur at a load $P_p$. As further predictions of the conventionally used girder theory, the web buckling load $P_{cr}$

and the computed cantilever end deflection $V_{th}$ are given. The computation of these reference values is given in Part 1, Secs. 1.5 to 1.7. They are tabulated together with the observed ultimate loads in Table 3.2.

There is little further description needed to interpret the information condensed into the figures of this section, since the load and web deflection curves are similar to the ones presented in Sec. 2.3 where they are discussed in detail. As is indicated, three tests were conducted on girder G6 and two on girder G7. The appearance of girder G6 after the first test is given in Fig. 3.5 and after the third in Fig. 3.6. Upon completion of the first test, the left hand panel was subdivided with one pair of stiffeners while in the right panel two pairs were added. This allowed a second test on the same girder, with an aspect ratio of $\alpha = 0.75$. After reinforcing with two diagonal stiffeners, a third test was conducted with $\alpha = 0.50$. It is possible that these two tests, T2 and T3 on girder G6, would have resulted in somewhat higher ultimate loads if conducted on panels with more favorable initial conditions. For girder G7, Figs. 3.7 and 3.8 are photographs of the test section after the first and second tests. The welding of a compression diagonal into the failed panel allowed the second test to be conducted.

While these photographs give an impression of the web distortions after their respective ultimate loads, the web deflection charts in Fig. 3.9 and Fig. 3.10 provide exact measurements of initial deflections and those near ultimate load. They also indicate the rate of increase of the web deflections and demonstrate the same fact as observed in the bending girders, namely that web buckling in the sense of the linear theory does not develop.

## 3.4 SR-4 Strain Gage Measurements

In this section strains as determined from SR-4 (A-1) gages on the web, the flanges, and the stiffeners are discussed. Although the SR-4 gage is a sensitive and valuable research tool, the resulting strains are easily misinterpreted; therefore, a more extensive presentation is necessary than is required for other topics. All of the considerations given here also apply to the other girders' strain observations.

Before going into detail, it will be helpful to review the following points about strain measurement with SR-4 gages.

Measured strains are actually obtained as the difference in resistance offered to an electric current. These changes in resistance must be caused entirely by lengthening or

shortening of the gages which are glued to the specimen. Temperature changes, which affect the gage's resistance, were eliminated by using a temperature compensating gage. In addition, it was attempted to complete a loading cycle as quickly as possible. When the cycle took a longer time than expected, in some cases as long as one-half a day, possible drifts in the recordings were carefully checked through the use of a "dummy" gage, which was mounted on a separate steel plate under no load and placed on the girder to conform to its temperature.

Since in a welded plate girder residual stresses are present, the recorded strains under load may differ greatly from the predicted ones. For most of the strain measurements presented in this report, this difficulty was eliminated by considering only those strains obtained in the second cycle of loading at loads between zero and the maximum load of the first cycle. The reasoning is illustrated in Fig. 3.11, where a likely state of residual stresses is shown and stresses due to applied bending moment are shown separately. In superimposing these two stress conditions, the compression flange stresses are as shown in the second row of the figure. It is obvious that the change of stress $\Delta\sigma$ is not uniform across the plate because $\sigma_y$ is first reached along the flange tips. Moreover,

due to redistribution of stresses to fulfill the equilibrium requirements the stresses at the center line of the plate is not simply $\sigma_r + \sigma_l$. That is, if a strain gage is mounted at this line, the strain recorded by the difference of gage readings will not equal to that caused by $\sigma_l$ alone. After reducing the applied load, the residual stresses take a new pattern with intensities along two sides of the flange reduced. For subsequent loadings within the magnitude of the previous cycle, no yielding happens, thus the measured and the computed stresses do agree with each other.

Finally, for the interpretation of the results, it must be kept in mind that all changes in strains are measured at the surface of a plate and thus are not necessarily representative of "the stress in the plate". If, for instance, Hooke's law and Navier-Bernoulli's assumption on the strain distribution in a plate girder should be checked, it would be absolutely necessary to measure strains on both surfaces of the web. For the web is a thin element and is susceptible to bending about its own axis, thus producing both membrane and bending strains on its surface. The average of surface strains on opposite sides, that is, the membrane strains, is the only value that could be expected to increase lineraly with the applied load and the distance from the neutral axis, and thus in a position to check the two stated assumptions. Fig. 3.12 illustrates what is defined as plate bending

stresses (sketch a) and membrane stresses (sketch b). Again, although a theory may only be concerned with one type of stresses, when experimenting with structures composed of steel plates one should always anticipate a stress or strain distribution as given in sketch C of Fig. 3.12.

Strain Rosettes on the Web of Girder G6

In order to obtain evidence of a tension field action and generally to prove that a rearrangement of stresses takes place in the web of a girder under high shear, the state of stress in the web of girder G6 was observed at three points in a cross section. From Fig. 3.13 it is seen that the cross section was located at X = +37.5 where three rosettes were placed, at Y = +21, 0, and -21. A photograph of the panel in which these rosettes were located is reproduced in Fig. 3.14.

From Fig. 3.13 the bending moment M and the shear force V under a jack load of 27 kips are M = 1013 k-in and V = 27k for the cross section at X = +37.5. With the moment of inertia I = 14,180 $in^4$, Table 1.6, and the static moments $Q_{21}$ = 257 and $Q_o$ = 300 $in^3$ for points 21 and 0 inches away from the neutral axis, respectively, the predicted stresses according to the beam theory would be:

| Location Y(=y) | Bending Stress $\sigma = \frac{M}{I} \cdot y$ | Shear Stress $\tau = \frac{VQ}{It}$ |
|---|---|---|
| +21 in | 1.500 ksi | 2.535 ksi |
| 0 in | 0.000 ksi | 2.959 ksi |
| -21 in | 1.500 ksi | 2.535 ksi |

For the loads of 54, 81, and 108 kips, the predicted strains would be 2, 3, and 4 times the values listed above. These theoretical values of principal stresses are drawn as dashed lines in Fig. 3.15, each one at its proper location.

Experimentally, the strains at the gages were recorded and the strains $\varepsilon_x$, $\varepsilon_\xi$, and $\varepsilon_\eta$ were computed (twelve gage readings are needed), as shown in the data sheet Fig. 3.16. The principal strains were then found by using Mohr's circle, Fig. 3.17. For the Mohr's circle construction see, for example, Ref. 276.

Knowing the magnitudes and directions of the principal strains, the vectors representing the principal stresses can easily be determined. The computations are carried out in Fig. 3.17 and the stress vectors drawn in their respective locations in Fig. 3.15. The differences between the theoretical and the experimental results are obvious.

Flange Strain Measurements

While Fig. 3.15 depicts the state of stress found in the web of girder G6, the results of strain measurements on its flanges are presented in Fig. 3.18. Here, the outline of the girder and the location of the strain gages mounted on the flanges in the panel extending from X = o to X = +75 are shown. The ordinate in the diagrams is flange strain or stress and the abscissa is the X coordinate plotted in the same scale as the girder's outline. The observed data are recorded and compared with the predictions of the beam theory as given by the dashed lines.

A similar graph for girder G7 is presented in Fig. 3.19. In this graph most readings follow the same trend as those for girder G6, the exceptions being those for load No. 18. A check with the load-deflection curve shows that this reading was taken after the ultimate load had been reached. At that stage secondary effects were so pronounced that the SR-4 strain readings were not representative of "flange strains". Cases like this happen very often in experimental investigations. Instead of omitting these data in the graph, an explanation for this peculiarity is presented below.

Beyond the ultimate load, the web plate stretched and deformed in a manner illustrated in Fig. 3.20 (also Fig. 3.7).

This action caused the flanges to bend. It is seen that in this figure the flange bending effect is more pronounced in the compression flange than in the tension flange because compression stresses contribute to the deformation and tensile stresses retard them. At any rate, the curvature introduced in each flange causes considerable plate bending stresses which are superimposed on the flange membrane stresses. Taking as an example the point X = +31, Y = -25 3/4 on the extreme fiber of the compression flange, (Fig. 3.19), the plate bending stress is tensile and the membrane stress is compressive, therefore, the total stress is expected to reduce in magnitude. This is indeed what the SR-4 gage recorded.

If the gage at X = +31, Y = -25 3/4 would have been mounted on the girder a few more inches closer to the panel center, the opposite effect would have occurred. For nearer to the panel center, plate compressive stresses would be added to compressive membrane stresses. Although no gages were mounted here, yield lines were observed on the compression flange surface as photograph taken at load No. 18 and presented in Fig. 3.21 shows. The ruler appearing in this photograph gives the distance from the girder's centerline, that is, the X coordinate distance. From this picture, it is evident that pronounced yielding occurred in the region near the panel center.

Strains in Transverse Stiffeners

As the third and last group of important measurements by SR-4 strain gages, those strains observed on the transverse stiffeners is presented. For girder G6 this is done with the help of Fig. 3.22 where the axial strain in the stiffener is plotted for two loading cycles, load No. 1 to 6 and load No. 8 to 14. The graph on the left is drawn for the stiffener at X = 0, that on the right for X = +75. Two gages were employed on each stiffener, hence four for each pair. The average of strains by these four gages are the axial strains plotted.

In order to bring out the importance of the average strain, the observations for the stiffener at X = +25 are presented in detail for girder G7. There, a total of six gages were arranged at the same elevation on the double-sided stiffener as Fig. 3.23b indicates. The reason for this layout was to find out whether or not the average of gages No. 25 and 26 would lead to the same average axial strain as obtained by averaging the four gages, Nos. 23, 24, 27, and 28.

The stiffener pair, if considered as a unit, is a prismatic bar with a rectangular cross section. Over this cross section, the recorded stresses are plotted in sketch c for load No. 5 and the whole stress block is indicated.

As seen, no one reading could be chosen as the representative one for the stiffener's axial stress.

Furthermore, the stress distribution at the next higher load, load No. 6, is entirely different from the one before, sketch d. The explanation of this behavior is readily understood if reference is made to the web deflection curve, Fig. 3.10. Here it is seen that a considerable change in the web deflection shape occurred between loads No. 5 and 8. A horizontal section through the web is given in Fig. 3.23a in which the web, changing its buckling pattern, also twists the stiffener. According to this sketch, alternate compression and tension in the corners of gages Nos. 23, 24, 28, and 27 must be superimposed on the average axial stress. This is certainly confirmed by the stress block shown in Fig. 3.23d.

The last sketch in this figure, Fig. 2.23e, gives the magnitude of the stresses at load No. 8 which follow quite closely the pattern observed at load No. 6. The sketch, rather than being an "oblique projection", is shown in a cavalier projection to preserve the relative dimensions of all parts. The question raised before concerning whether or not gages Nos. 25 and 26 could replace the other four can now be answered. Theoretically it is possible, but practically it cannot be done. This is due to the fact that

the SR-4 strain gage, with its resistance wires spread over a width of one-eighth inch, cannot truly be centered on the one-quarter inch plate edge. A mere shift of one-sixty fourth of an inch from center would mean an error in the stress reading of about 3 ksi at Z = +4 3/32 for load No. 8.

Finally, the strain readings of each individual gage are plotted in Fig. 3.24 together with the average as computed from the four gages on the stiffener's sides. Again it should be emphasized at this point that all stiffener readings presented in this investigation are the average of these four gages. In this figure is seen a classical example of how SR-4 gages can give misleading results if the points mentioned in the introduction to this section are not considered.

## 3.5 Additional Strain Measurements

### Whittemore Gage Readings

Since the use of the electrical SR-4 gages is essentially confined to the elastic range of the material, a mechanically operated Whittemore gage was also used to obtain web deformations. This gage records the change in distance between two gage points. A photograph of the layout of these points as used for girder G6 appears in Fig. 3.14 and the centerline of the three rows is again drawn in Fig. 3.25 where the resulting strains are plotted.

In this latter figure, the strains are given for three loads, Nos. 3, 5, and 13, plotted in the direction of measurement. The yield strain $\varepsilon_y$ is also indicated as a reference. Similar graphs are presented as Fig. 3.26 and Fig. 3.27 for girder G7. In Fig. 3.27 the scale is changed because the strains are multiples of the yield strain.

The Whittemore gage used had a smallest dial division of one ten-thousandth of an inch, well below the "yield reading" which was computed as the product of the gage length and the yield strain: $3.5 \times 36.7/30{,}000 = 0.0043$ inches. Of course, this does not reflect the accuracy of the given results, since repetitive measurements differed in most cases by several ten-thousandths of an inch. Thus, three readings were taken for each elongation measurement and the resulting average strain is plotted. Statistically the standard deviation of a plotted average value is evaluated at about 3 ten-thousandths of an inch, or about 7% of the yield reading.* Therefore, it is justifiable to use these figures for a tension field evaluation in the elastic range.

---

* The standard deviation for the individual readings, computed from all the 3 readings, is about 3.5 ten-thousandths of an inch. The standard deviation of the average of a set of three readings, therefore, is $3.5 \times 10^{-4}/\sqrt{3}$ inches.

Since the figure contains only differences between readings, the standard deviation of these differences plotted in the figures is $\sqrt{2}\,\frac{3.5}{3} \times 10^{-4} \approx 3 \times 10^{-4}$ inches which amounts to a coefficient of variation of about seven percent.

Corner Dial Readings

In an effort to observe the integral action of the web panels under high shear, AMES-dials were used. They were secured to clip angles spot welded to the web at the corners where a relatively fixed position could be maintained. The layout of these dial gages is indicated in Fig. 3.14, where it is seen that longitudinal, transverse, and diagonal panel distances were measured. With dials in all panels of the test section, an interrelated system of measurements could be taken such that the location of all panel corner points would be known with respect to some fixed datum. The datum chosen for girder G6 was the vertical line at X = 0. With an antisymmetrical loading, this line remains vertical and, with a stiffener at this location the distance between its end points remains essentially fixed. Therefore, a Williot-Mohr graphical solution to obtain the position of the panel corner points was used.

The results of this construction are given in Fig. 3.28 which shows the distorted test section of girder G6 in an exaggerated scale. While the dots indicate the results of

four loads, load Nos. 9, 10, 11, and 12, only the results of the most pronounced case occurring at the ultimate load, load No. 12, are connected by the solid lines. For comparison, the theoretical deformations of this section due to bending and shear are given for the same load by the dashed lines. It is easily seen that the longitudinal deformations due to bending were about the same as predicted but the vertical desplacements due to shear exceeded their predicted values. As shown in Fig. 3.28, lengthening occurred in one diagonal direction and shortening in the other.

## 3.6 Discussion

The experiments on the two shear girders were planned to verify the existence of a tension field or stress action. Some of the presented graphs will now be reviewed with the purpose of showing that this phenomenom did develop.

The web deflection drawing for girder G6, Fig. 3.3, illustrates that under increasing load a valley gradually forms which extends from the lower left corner of a panel to the upper right. This is the direction of the tension diagonal. The same tendency can be observed in girder G7, Fig. 3.4, although it is somehwat less obvious with only three cross sectional recordings per panel.

In order to obtain an insight into the state of stress, Fig. 3.15 was prepared. The figure compares the measured principal stresses with the ones computed according to beam theory. At mid-depth of the panel pure shear should be recorded, that is, equal magnitude in principal tension and compression stresses. But at a load P = 27 kips, which is about equal to the computed critical load, the principal tension stress is somewhat higher than predicted, while the principal compressive stress is smaller. At two, three, and four times this load the observed tendency becomes even more pronounced. Furthermore, the inclination of the principal tension stress changes gradually, starting at about $45^{\circ}$ and decreasing to a smaller value.

The two rosettes placed close to the tension and compression flanges, at y = +21 and y = -21, show less deviation from straight beam action. It is interesting to see that these rosettes also differ in behavior. This difference between the top and the bottom of the girder is even more pronounced when Fig. 3.18 is considered. The figure represents the strain readings at the extreme fibers of the flanges. While the stresses in the top flange at X = +37 1/2 inches are consistently below the ones predicted by beam theory, the compression stresses in the bottom flange are above the predicted values. With the help of Fig. 3.20 this can be interpreted. Considering girder G6 as a Pratt-

or N-type truss, that is, having only tension diagonals, the flange force in the top chord of the panel X = 0 to X = +75 would be equal to the moment at X = 0 divided by the girder depth. The force in the lower chord would be obtained from the moment at X = +75, which is certainly higher in magnitude than at X = 0. The flange stresses do exhibit a tendency toward truss action. The net result is neither a straight line stress variation corresponding to beam action nor a constant stress of pure truss action but a combination of the two as shown in Fig. 3.18. This same tendency can be observed from Fig. 3.19, which contains the corresponding graph obtained from girder G7, as well as from other types of measurements such as the recorded overall panel distortions, Fig. 3.28.

From the Whittemore gage observations, Figs. 3.25, 3.26, and 3.27, it is seen that the web portion under tension is wider than generally expected. This serves as a explaination for the obtained ultimate loads which are at least 200% higher than $P_{cr}$ and cannot possibly be due to a narrow tension diagonal when considering the yield strength of the web material. Therefore, instead of using the words truss action and tension diagonal, it shall henceforth be termed tension field action and tension field, respectively.

The most positive indication of tension field action is the observation of axial stresses in the transverse stiffeners. The test evidence presented in Sec. 3.4 shows clearly that at loads beyond $P_{cr}$ a stiffener picks up axial load. The magnitude of this stiffener force cannot very well be determined because the web's participation in carrying the tension field force is unknown. But a simple strength evaluation of the web, with some equilibrium considerations, help to close the gap. For this, reference is made to the theoretical study which paralleled this investigation, Ref. 7.

In summary, the tests on the two shear girders of high web slenderness ratios revealed that in girders subjected to shear a considerable post buckling strength exists. In one case, first test of girder G6, the ultimate load was four times the computed shear buckling load. The explanation for post buckling strength is that a very pronounced tension field action develops due to the presence of transverse stiffeners.

Table 3.1

Weld Sizes
(Leg in inches)

| Girder | Flange to Web | | Inter. Stiffener to Web | | Load Stiffener to Web |
|---|---|---|---|---|---|
| | Test Section | End Section | Test Section | End Section | |
| G1 | 3/16 | 1/4 | 3/16 | 3/16 | 1/4 |
| G2 | 3/16 | 1/4 | 3/16 | 3/16 | 1/4 |
| G3 | 3/16 | 1/4 | 3/16 | 3/16 | 1/4 |
| G4 | 3/32* | 1/4 | 3/32* | 3/16 | 1/4 |
| G5 | 3/32* | 1/4 | 3/32* | 3/16 | 1/4 |
| G6 | 1/8* | 1/4 | 1/8* | 3/16 | 1/4 |
| G7 | 1/8* | 1/4 | 1/8* | 3/16 | 1/4 |
| E1 | 1/4 | | 3/16 | | 1/4 |
| E2 | 1/4 | | 3/16 | | 1/4 |
| E4 | 1/4 | | 3/16 | | 1/4 |
| E5 | 1/4 | | 3/16 | | 1/4 |
| G8 | 1/8* | | 1/8* | | 1/8* |
| G9 | 3/32* | | 3/32* | | 3/32* |

* Not submerged arc welding

Table 3.2

Summary of Reference and Experimental Loads

| Girder | Test | Theoretical | | | Experimental | |
|---|---|---|---|---|---|---|
| | | $P_{cr}$ (kips) | $P_y$ (kips) | $P_p$ (kips) | $P_u$ (kips) | $P_{max.}$ (kips) |
| G6 | T1 | 27.4 | 193 | 205 | 116 | 119 |
| | T2 | 51.9 | 193 | 205 | 150 | 151 |
| | T3 | 97.6 | 193 | 205 | 177 | 180 |
| G7 | T1 | 37.6 | 196 | 208 | 140 | 149 |
| | T2 | 37.6 | 196 | 208 | 145 | 150 |

Fig. 3.1 Plate Girders G6 & G7 with Test Setup

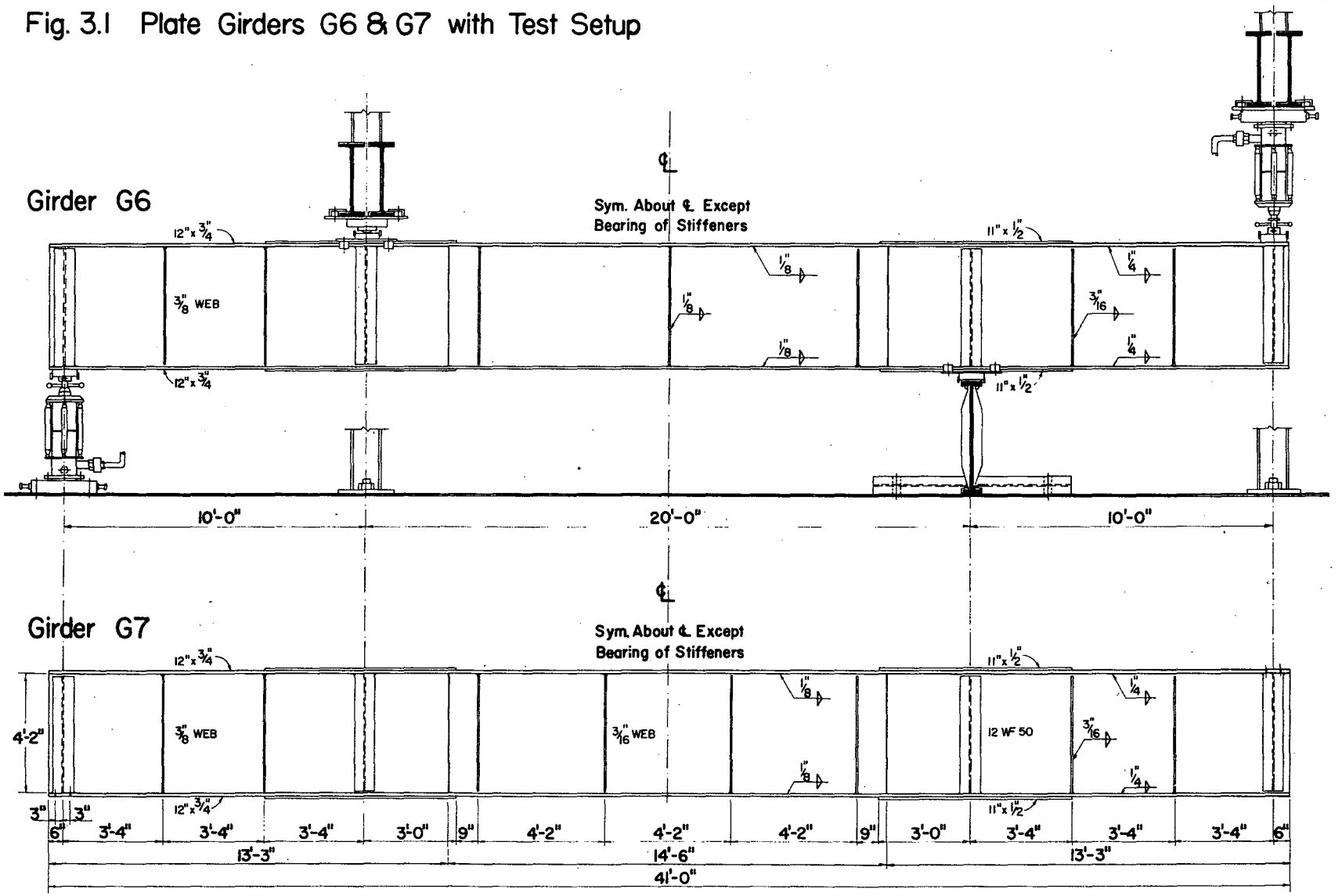

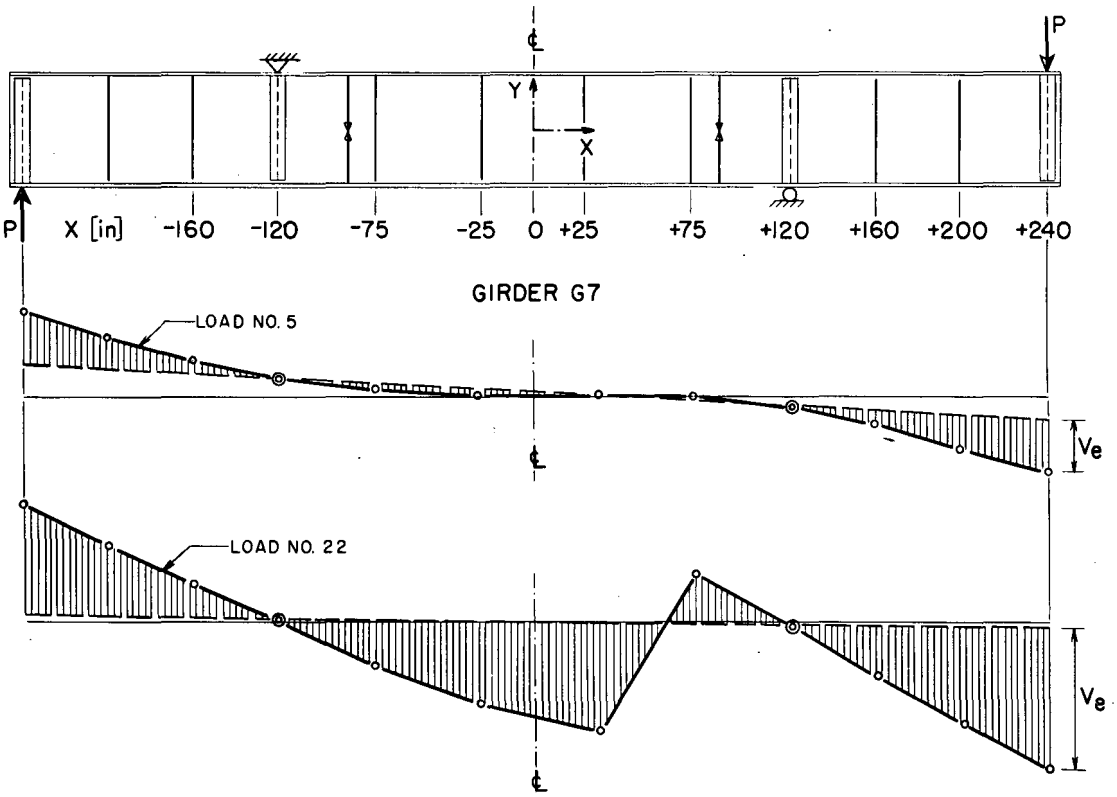


Fig. 3.2 Deflection Lines of Girder G7

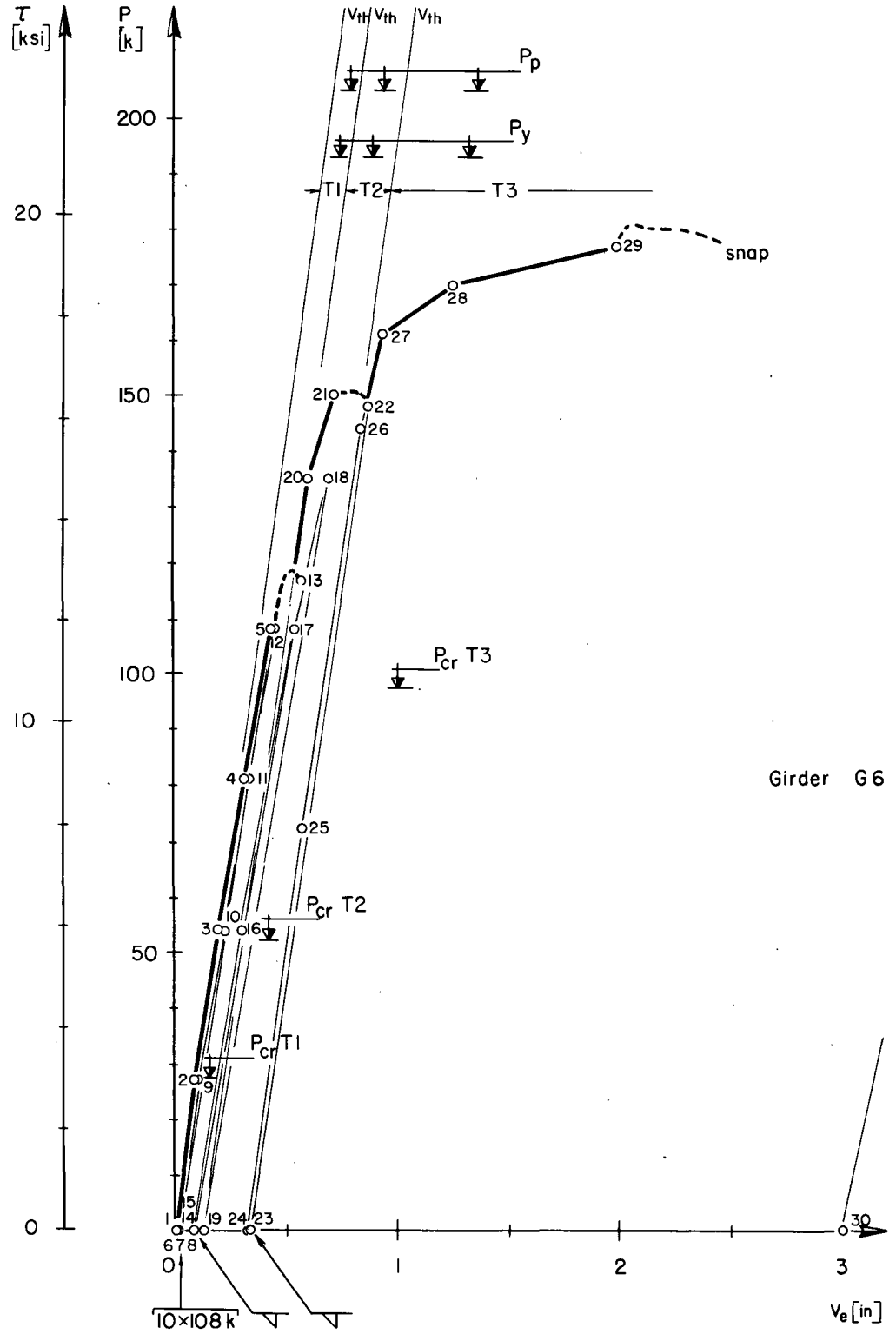


Fig. 3.3 Load-Deflection Curve, Girder G6

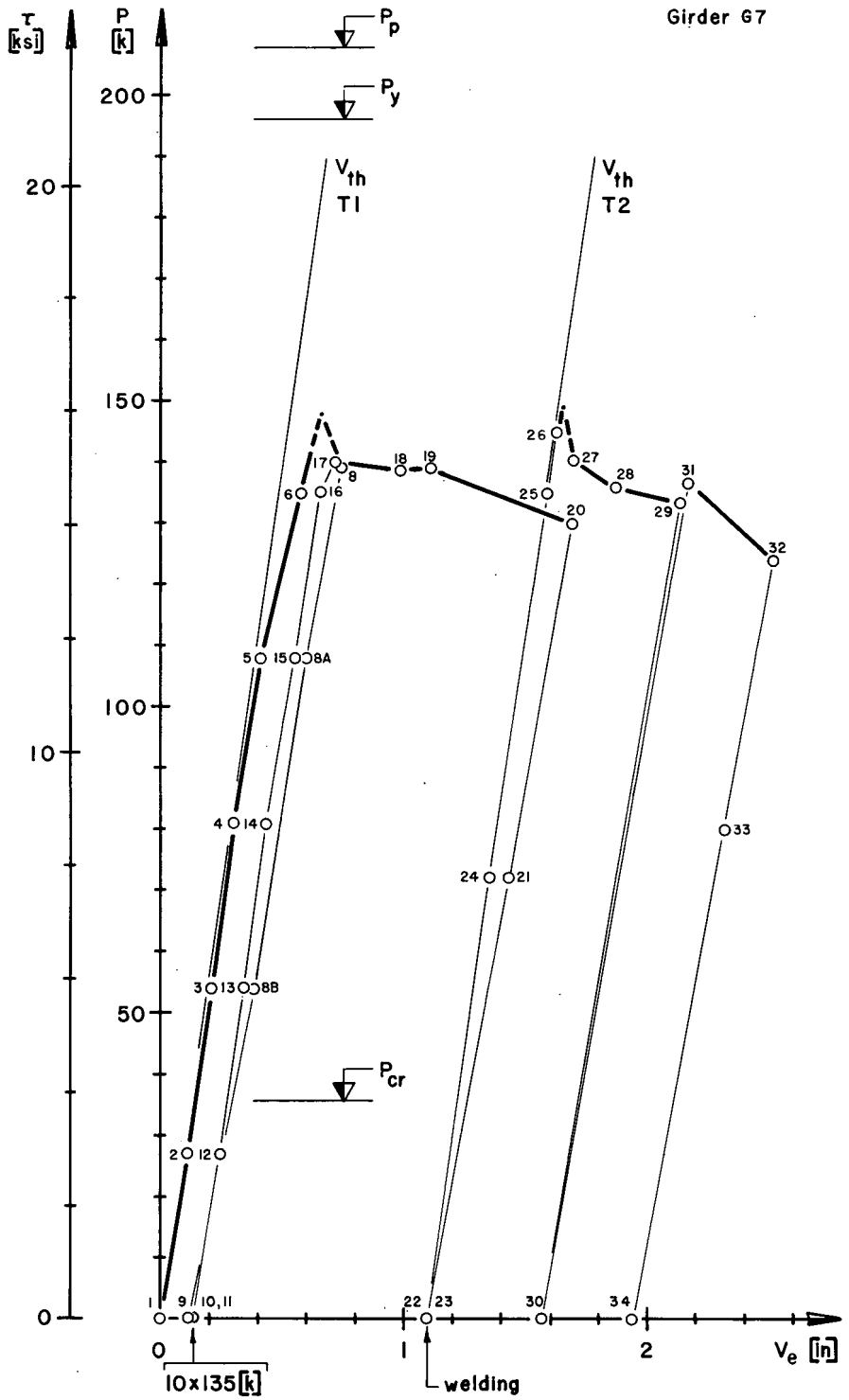


Fig. 3.4 Load-Deflection Curve, Girder G7

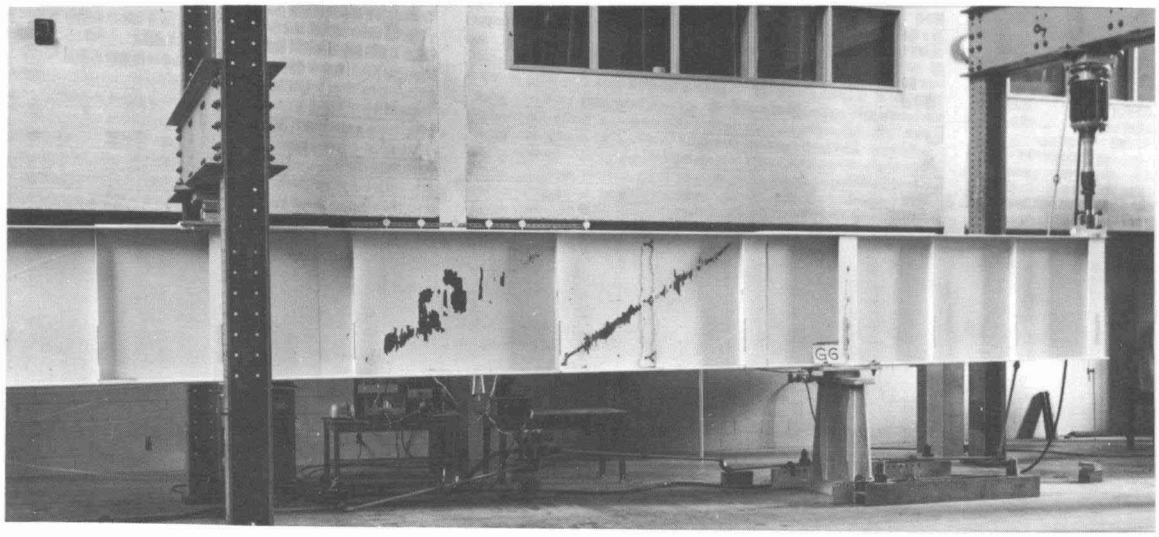


Fig. 3.5 Girder G6 after Test T1

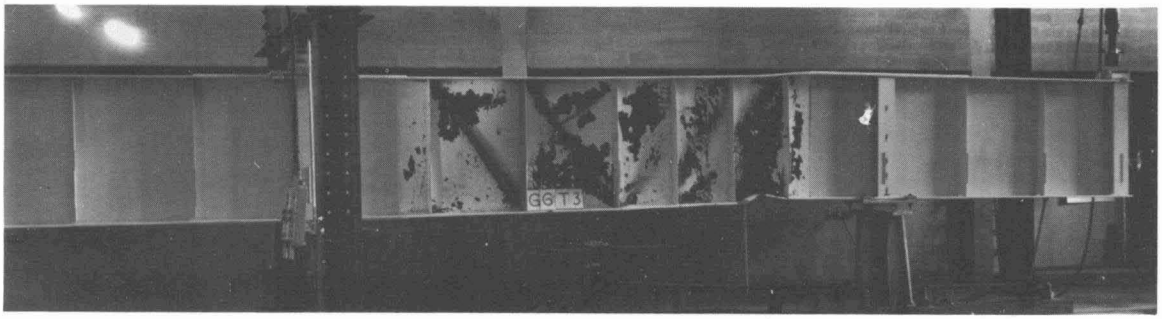


Fig. 3.6 Girder G6 after Test T3

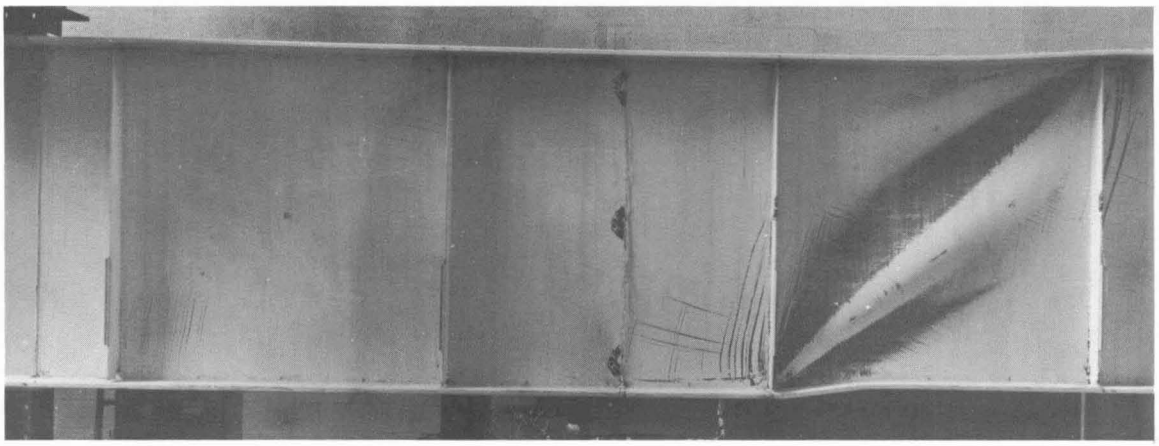

Fig. 3.7 Girder G7 after Test T1

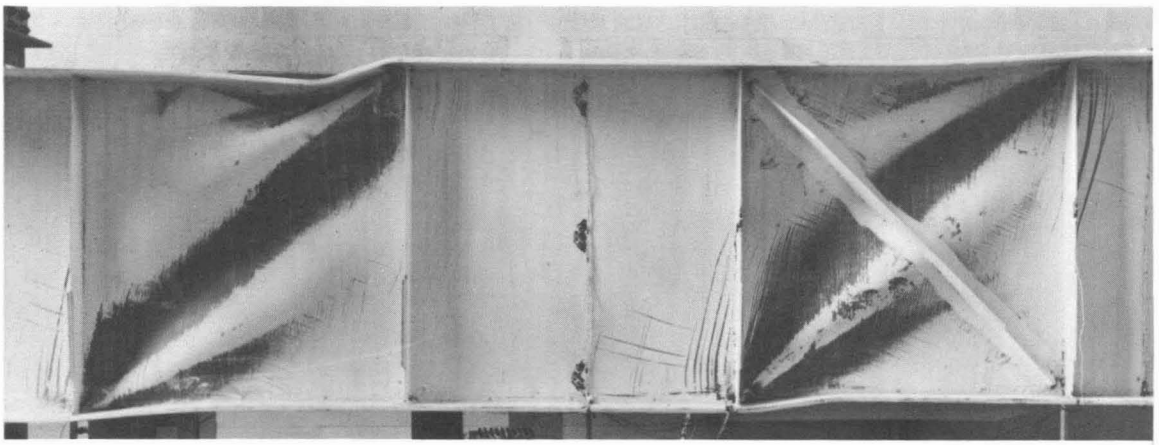

Fig. 3.8 Girder G7 after Test T2

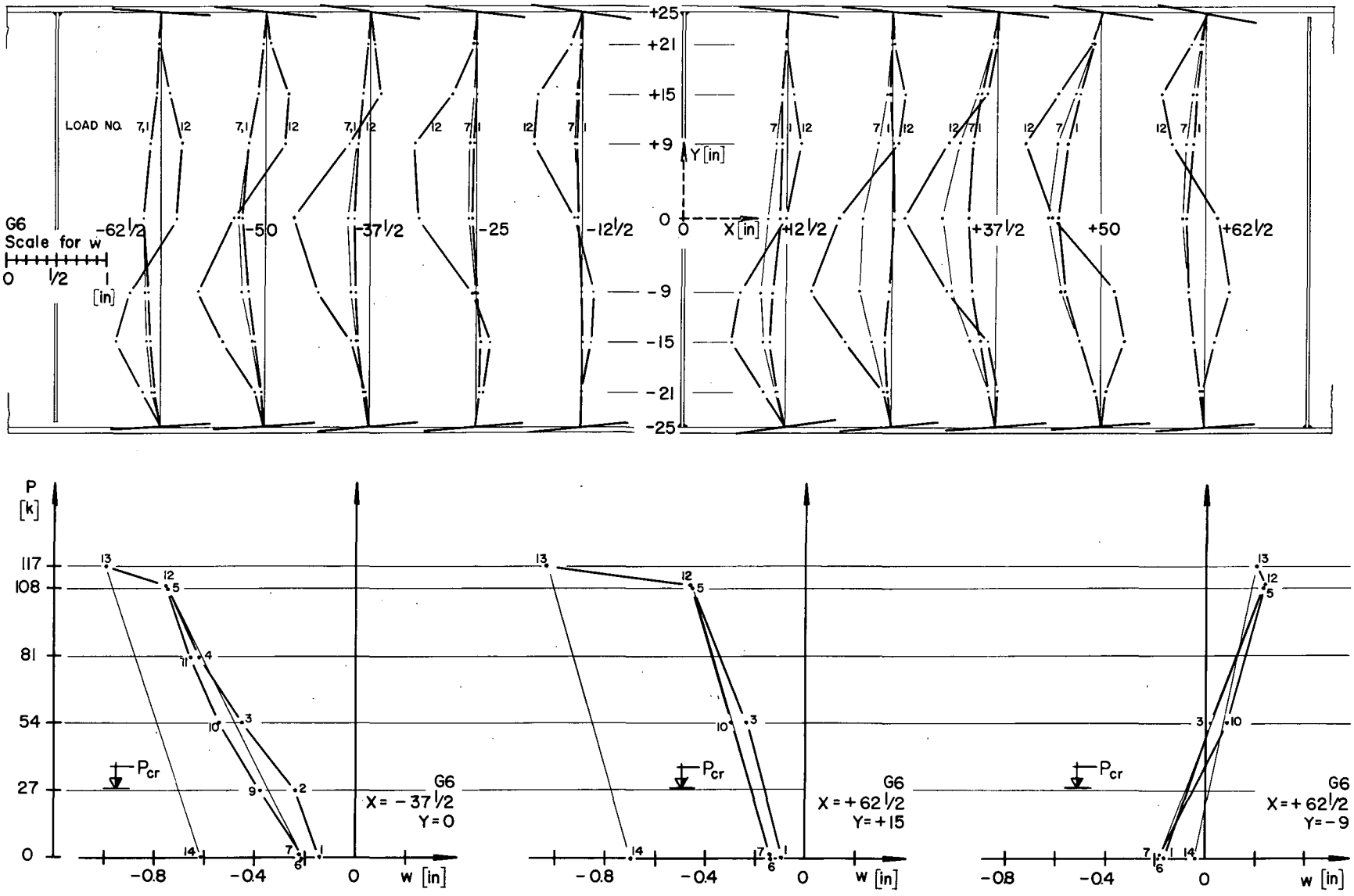


Fig. 3.9 Web Deflections of Girder G6

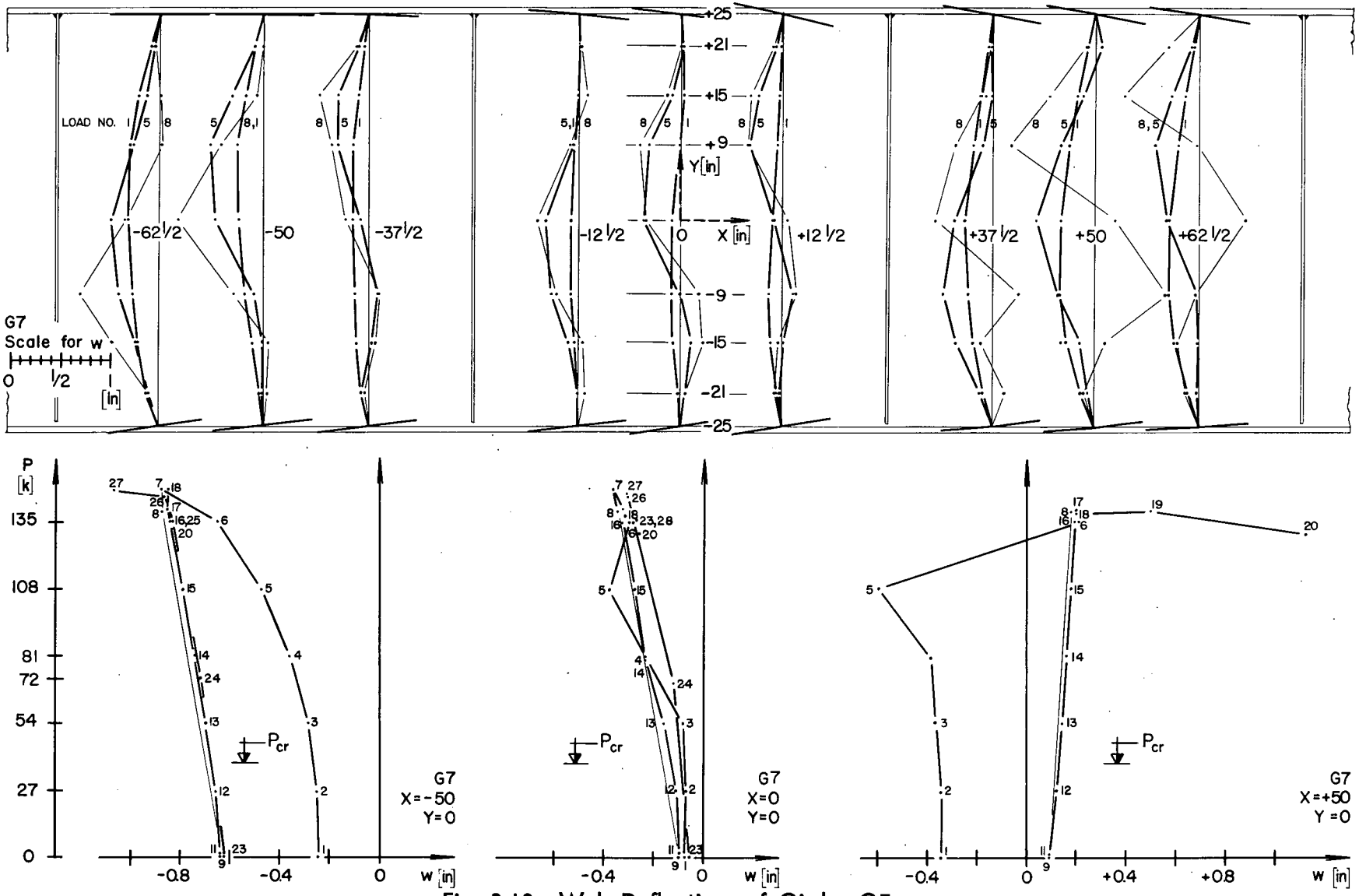


Fig. 3.10 Web Deflections of Girder G7

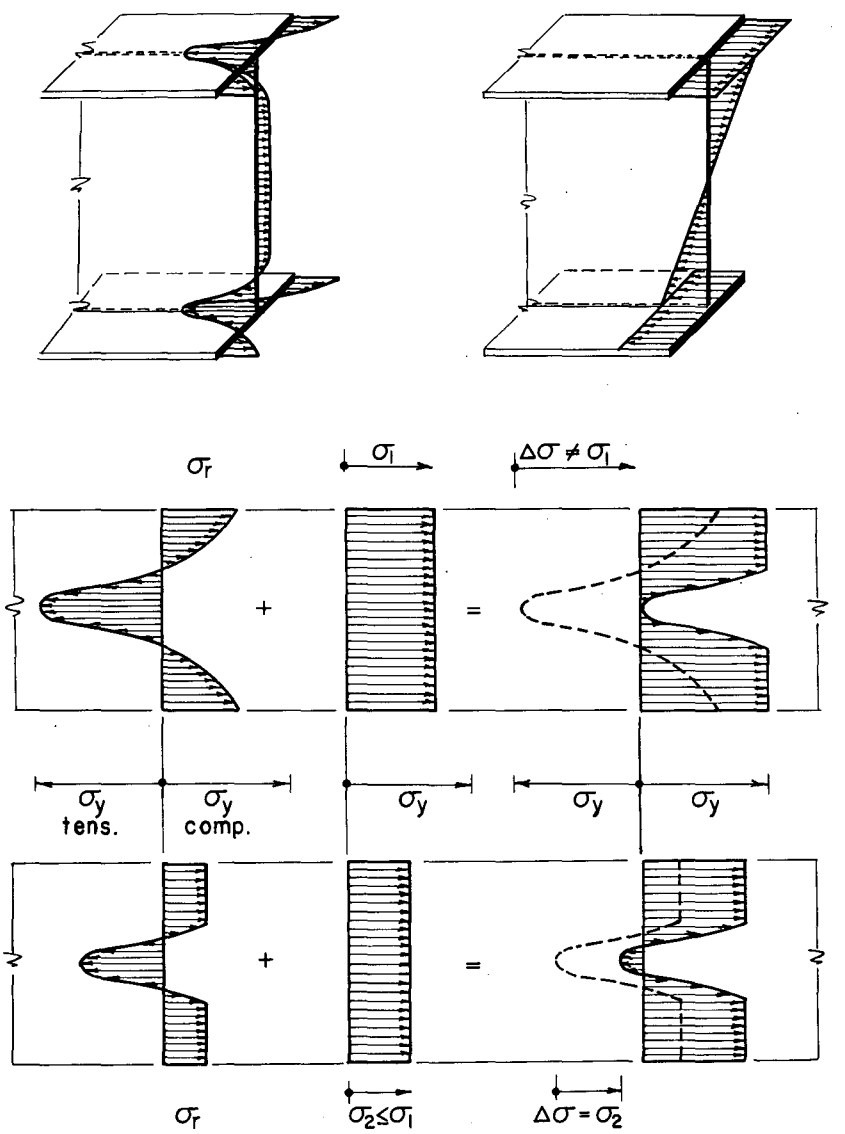


Fig. 3.11 Influence of Residual Stresses on Measurements

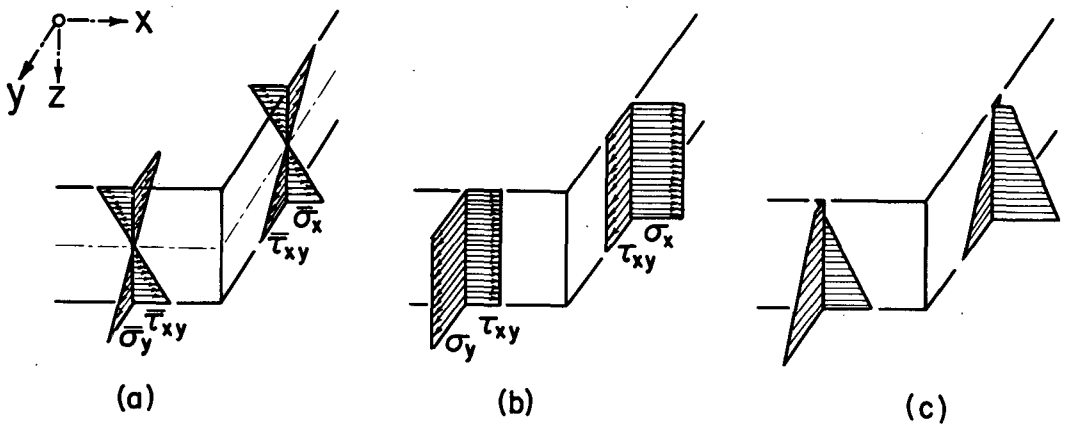


Fig. 3.12 Bending Stresses (a) and Membrane Stresses (b) in a Plate

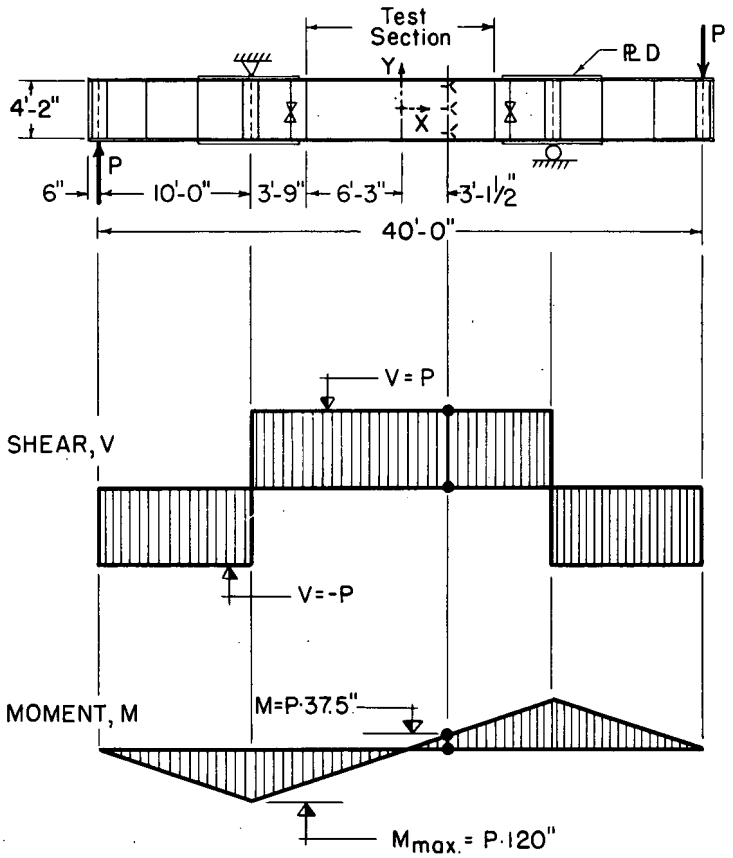


Fig. 3.13 Locations of SR-4 Strain Rosettes, Girder G6

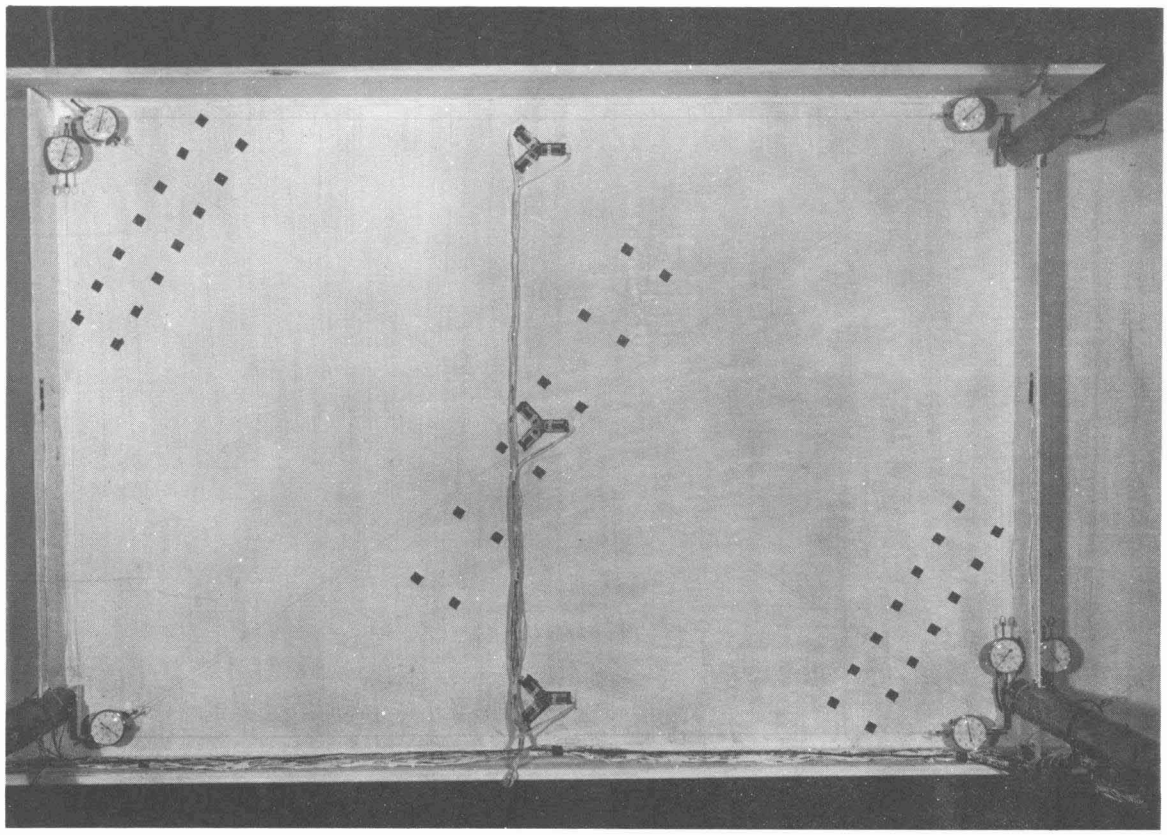

Fig. 3.14 Instrumentation of Girder G6

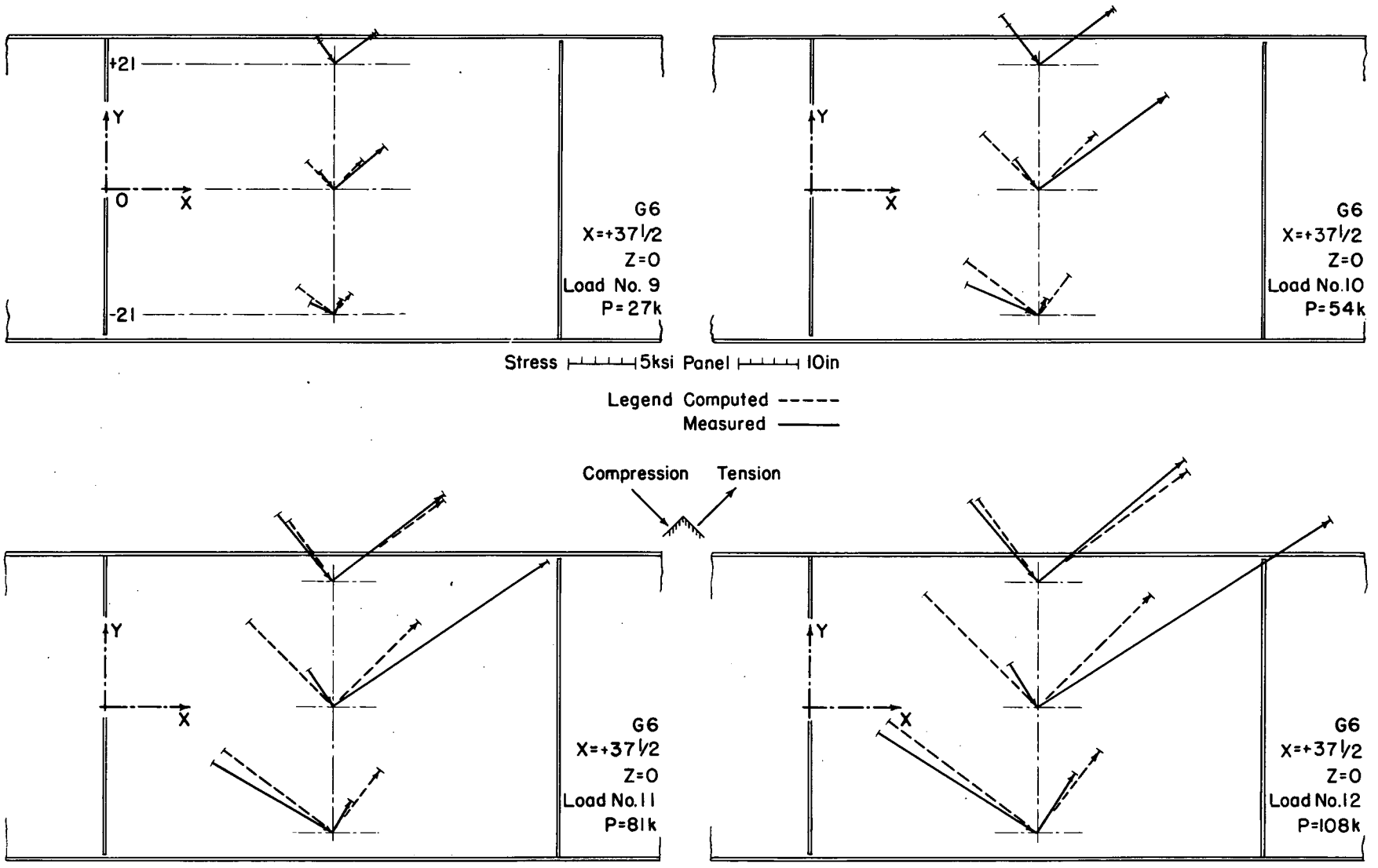


Fig. 3.15 Principal Stresses in Web of Girder G6

Subject: Strain Rosettes, SR-4 (A-1) Gages  Legend: R = Reading, D = Difference, ε = Normal Strain } In Microinches per inch.  Date: October 6, 1958

Specimen & Location: G6 T1 Web X = +37½  Name: B.T. Yen.

Note: Gage Factor 2.03, Strain Indicator FLA114

| Load No. | Load P [K] | Gage ⑨ R | Gage ⑨ D=R-R8 | Gage ⑩ R | Gage ⑩ D=R-R8 | $\varepsilon_x = \frac{D_9 + D_{10}}{2}$ | Gage ⑪ R | Gage ⑪ D=R-R8 | Gage ⑫ R | Gage ⑫ D=R-R8 | $\varepsilon_1 = \frac{D_{11} + D_{12}}{2}$ | Gage ⑬ R | Gage ⑬ D=R-R8 | Gage ⑭ R | Gage ⑭ D=R-R8 | $\varepsilon_1 = \frac{D_{13} + D_{14}}{2}$ | Remark |
|---|---|---|---|---|---|---|---|---|---|---|---|---|---|---|---|---|---|
| 8 | 0 | 7309 | | 12635 | | | 7597 | | 12911 | | | 6900 | | 12219 | | | |
| 9 | 27 | 7370 | +61 | 12660 | +25 | +43 | 7670 | +73 | 13130 | +219 | +146 | 6859 | -41 | 12029 | -190 | -115 | Rosette at Y=+21 |
| 10 | 54 | 7419 | +110 | 12673 | +38 | +74 | 7766 | +169 | 13290 | +379 | +274 | 6859 | -41 | 11822 | -397 | -219 | |
| 11 | 81 | 7467 | +158 | 12693 | +58 | +108 | 7880 | +283 | 13444 | +533 | +408 | 6871 | -29 | 11623 | -596 | -312 | |
| 12 | 108 | 7523 | +214 | 12722 | +87 | +150 | 7998 | +401 | 13598 | +687 | +544 | 6876 | -24 | 11449 | -770 | -397 | |

| Load No. | Load P [K] | Gage ⑮ R | Gage ⑮ D=R-R8 | Gage ⑯ R | Gage ⑯ D=R-R8 | $\varepsilon_x = \frac{D_{15} + D_{16}}{2}$ | Gage ⑰ R | Gage ⑰ D=R-R8 | Gage ⑱ R | Gage ⑱ D=R-R8 | $\varepsilon_1 = \frac{D_{17} + D_{18}}{2}$ | Gage ⑲ R | Gage ⑲ D=R-R8 | Gage ⑳ R | Gage ⑳ D=R-R8 | $\varepsilon_1 = \frac{D_{19} + D_{20}}{2}$ | |
|---|---|---|---|---|---|---|---|---|---|---|---|---|---|---|---|---|---|
| 8 | 0 | 8055 | | 12498 | | | 6653 | | 12347 | | | 6245 | | 13228 | | | |
| 9 | 27 | 8032 | -23 | 12654 | +156 | +66 | 6856 | +203 | 12509 | +162 | +182 | 5898 | -347 | 13367 | +139 | -104 | Rosette at Y=0 |
| 10 | 54 | 8014 | -41 | 12951 | +453 | +206 | 7068 | +415 | 12761 | +414 | +414 | 5411 | -834 | 13662 | +434 | -200 | |
| 11 | 81 | 8050 | -5 | 13270 | +772 | +383 | 7270 | +617 | 13008 | +662 | +639 | 4961 | -1284 | 13984 | +756 | -264 | |
| 12 | 108 | 8118 | +63 | 13595 | +1097 | +580 | 7480 | +827 | 13270 | +923 | +875 | 4518 | -1727 | 14299 | +1071 | -328 | |

| Load No. | Load P [K] | Gage ㉑ R | Gage ㉑ D=R-R8 | Gage ㉒ R | Gage ㉒ D=R-R8 | $\varepsilon_x = \frac{D_{21} + D_{22}}{2}$ | Gage ㉓ R | Gage ㉓ D=R-R8 | Gage ㉔ R | Gage ㉔ D=R-R8 | $\varepsilon_1 = \frac{D_{23} + D_{24}}{2}$ | Gage ㉕ R | Gage ㉕ D=R-R8 | Gage ㉖ R | Gage ㉖ D=R-R8 | $\varepsilon_1 = \frac{D_{25} + D_{26}}{2}$ | |
|---|---|---|---|---|---|---|---|---|---|---|---|---|---|---|---|---|---|
| 8 | 0 | 6450 | | 12181 | | | 8170 | | 9952 | | | 5757 | | 12991 | | | |
| 9 | 27 | 6389 | -61 | 12127 | -54 | -57 | 8148 | -22 | 10058 | +106 | +42 | 5815 | +58 | 12799 | -192 | -67 | Rosette at Y=-21 |
| 10 | 54 | 6280 | -170 | 12035 | -146 | -158 | 8032 | -138 | 10222 | +270 | +66 | 5843 | +86 | 12559 | -432 | -173 | |
| 11 | 81 | 6248 | -202 | 11917 | -264 | -233 | 8103 | -67 | 10340 | +388 | +160 | 5736 | -21 | 12332 | -659 | -340 | |
| 12 | 108 | 6243 | -207 | 11827 | -354 | -280 | 8270 | +100 | 10411 | +459 | +279 | 5568 | -189 | 12226 | -765 | -477 | |

Fig. 3.16 Typical Data Sheet for Strain Measurements with SR-4 (A-1) Gages

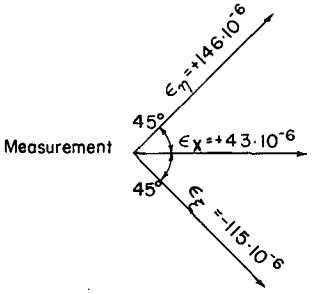


Principal Strains

$\epsilon_1 = +149 \cdot 10^{-6}$ in/in

$\epsilon_2 = -118 \cdot 10^{-6}$ in/in

Principal Stresses

$\sigma_1 = \frac{E}{1-\nu^2}(\epsilon_1 + \nu\epsilon_2) = +3.75$ ksi

$\sigma_2 = \frac{E}{1-\nu^2}(\epsilon_2 + \nu\epsilon_1) = -2.42$ ksi

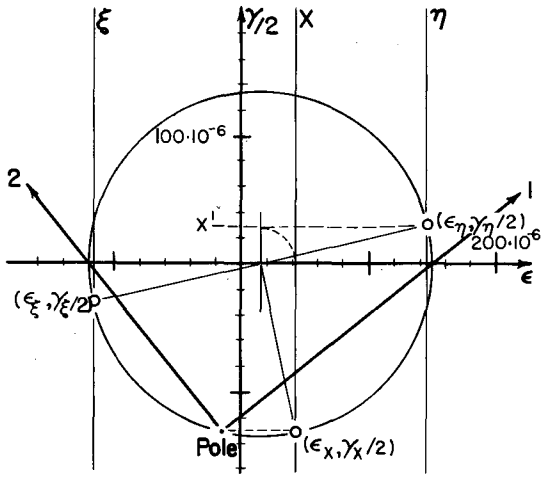


G6
X=+37 1/2
Y=+21
Z=0
Load No.9
P=27k

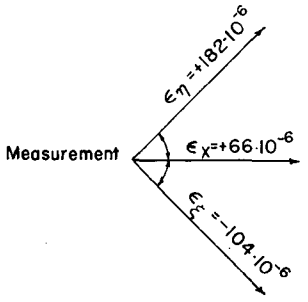


Principal Strains

$\epsilon_1 = +184 \cdot 10^{-6}$ in/in

$\epsilon_2 = -106 \cdot 10^{-6}$ in/in

Principal Stresses

$\sigma_1 = \frac{E}{1-\nu^2}(\epsilon_1 + \nu\epsilon_2) = +5.02$ ksi

$\sigma_2 = \frac{E}{1-\nu^2}(\epsilon_2 + \nu\epsilon_1) = -1.68$ ksi

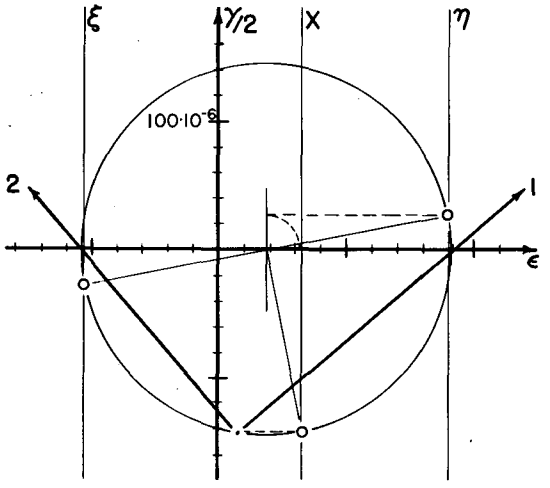


G6
X=+37 1/2
Y=0
Z=0
Load No.9
P=27k

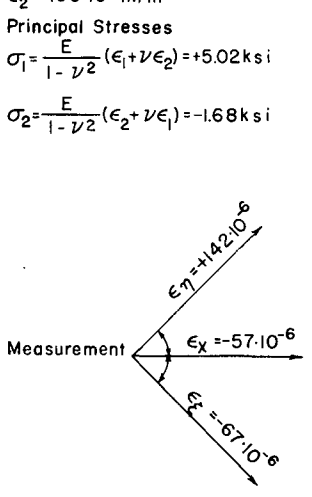


Principal Strains

$\epsilon_1 = +58 \cdot 10^{-6}$ in/in

$\epsilon_2 = -83 \cdot 10^{-6}$ in/in

Principal Stresses

$\sigma_1 = \frac{E}{1-\nu^2}(\epsilon_1 + \nu\epsilon_2) = +1.09$ ksi

$\sigma_2 = \frac{E}{1-\nu^2}(\epsilon_2 + \nu\epsilon_1) = -2.17$ ksi

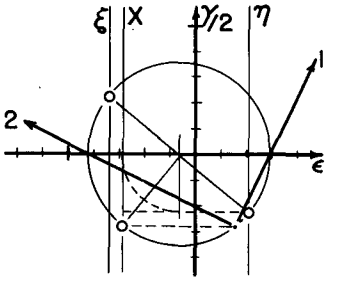


G6
X=+37 1/2
Y=-21
Z=0
Load No.9
P=27k

Fig. 3.17 Mohr's Circles for Strain Rosettes

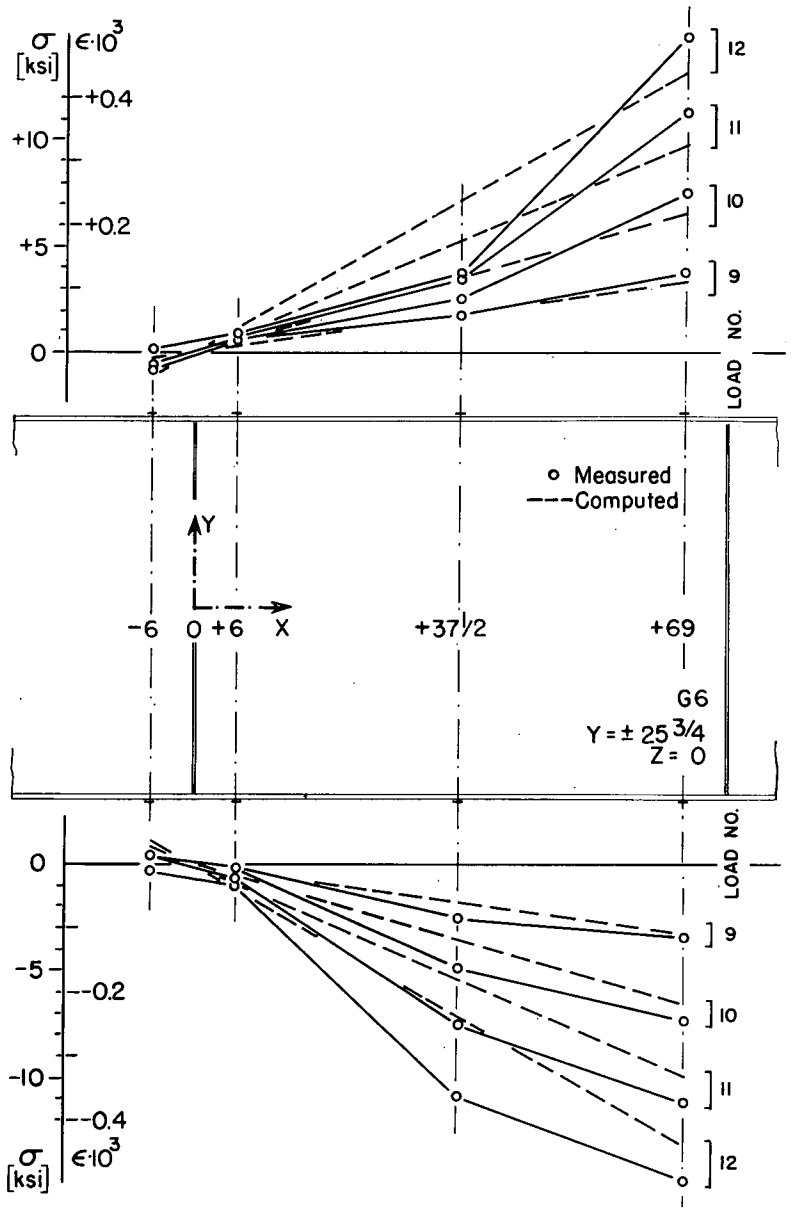


Fig. 3.19 Flange Stresses, Girder G7

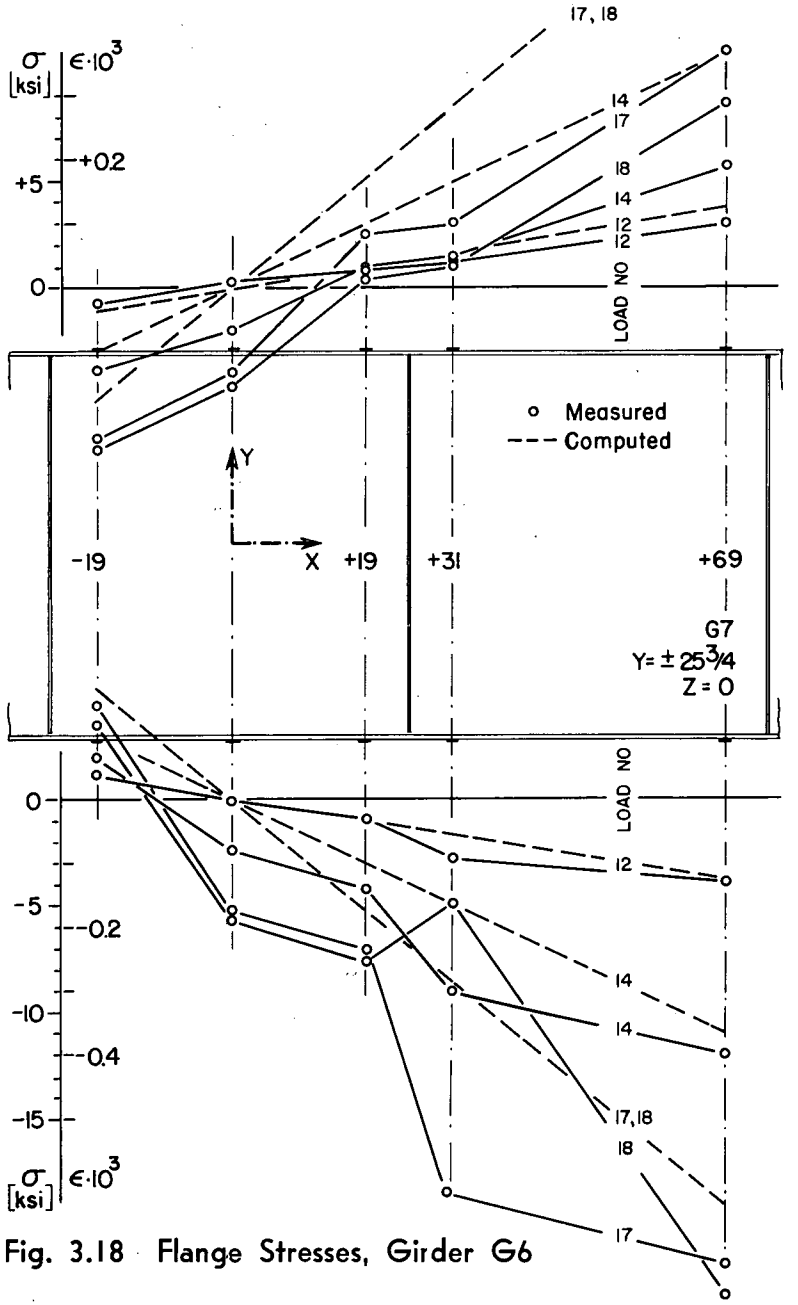


Fig. 3.18 Flange Stresses, Girder G6

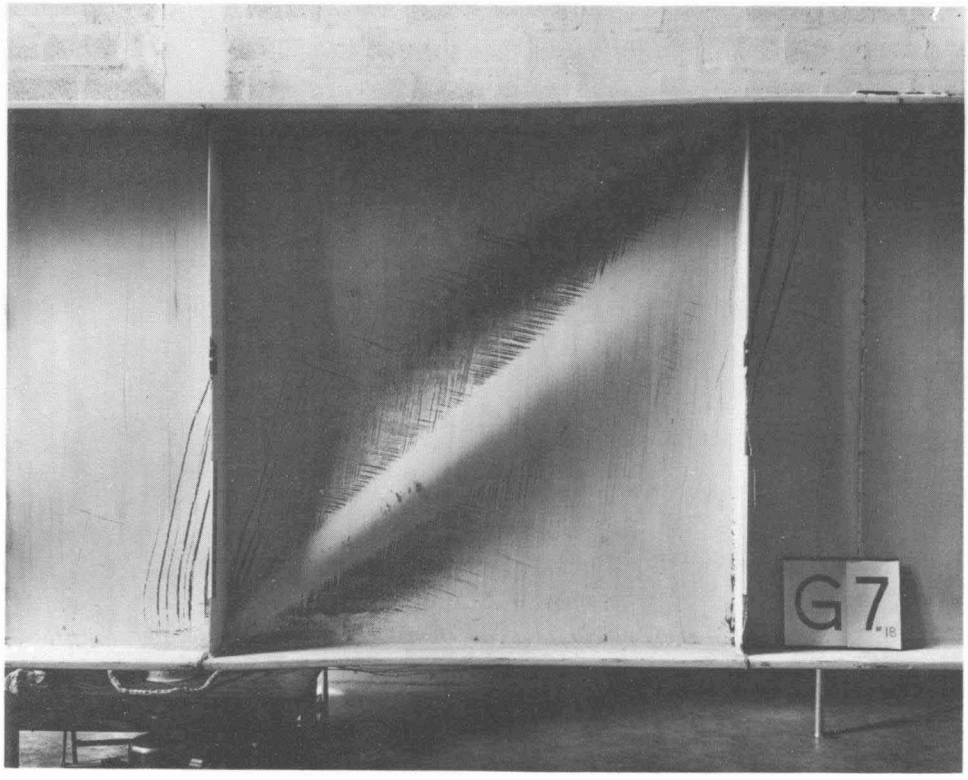


Fig. 3.20 Deformation of Flanges and Web after Ultimate Load, G7, Ti

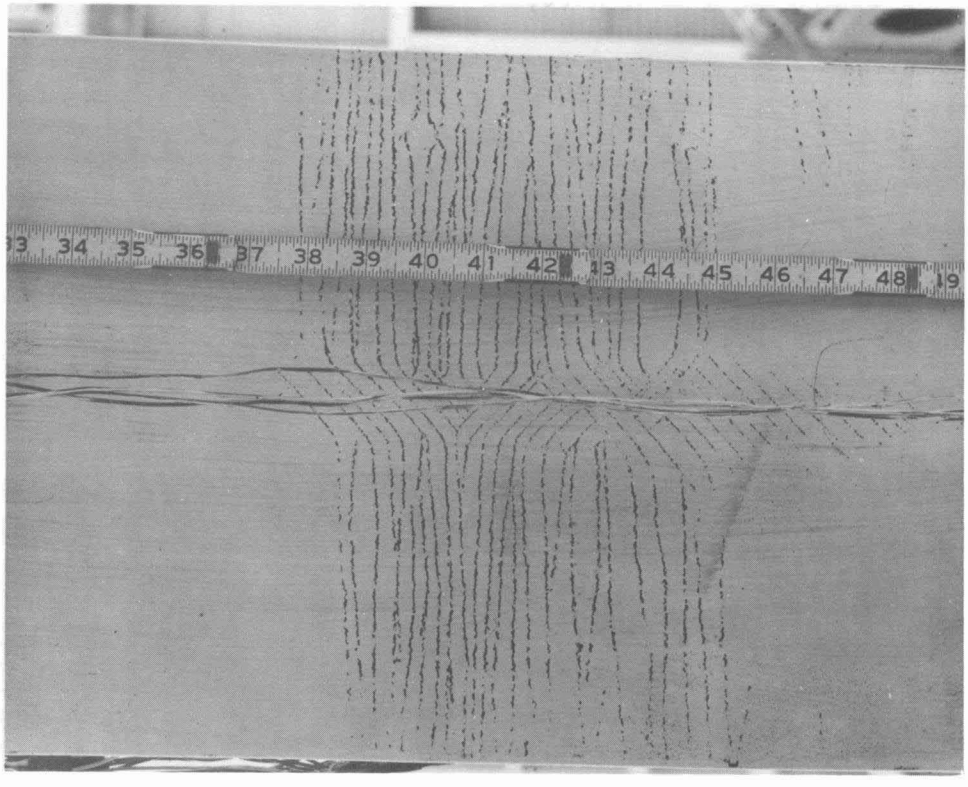


Fig. 3.21 Yield Lines on Bottom Flange after Ultimate Load, G7, TI

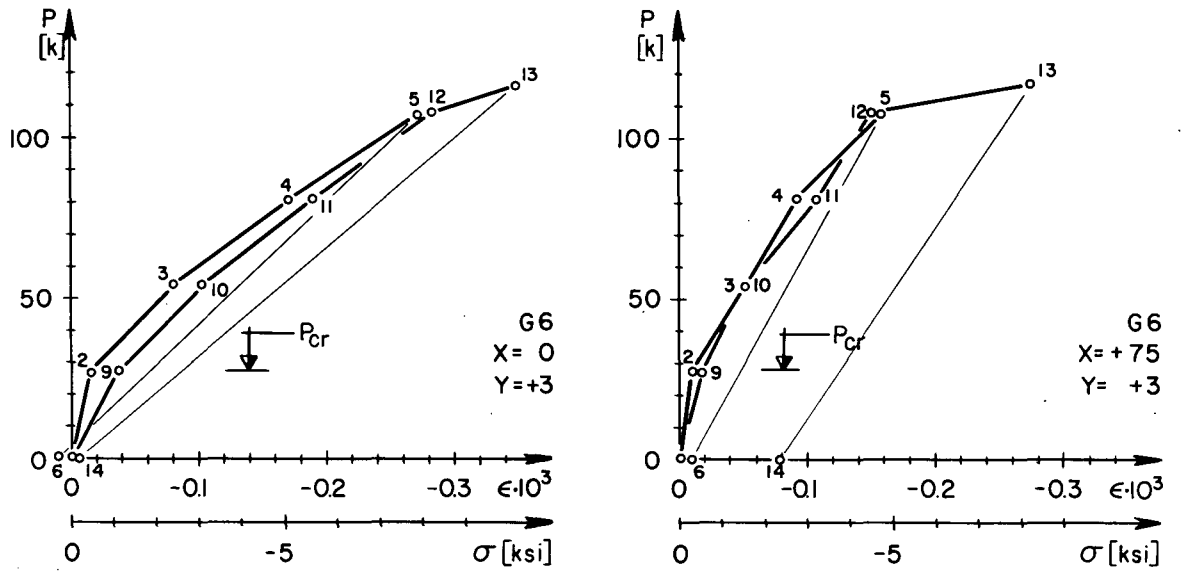


Fig. 3.22 Axial Strain in Transverse Stiffeners, Girder G6

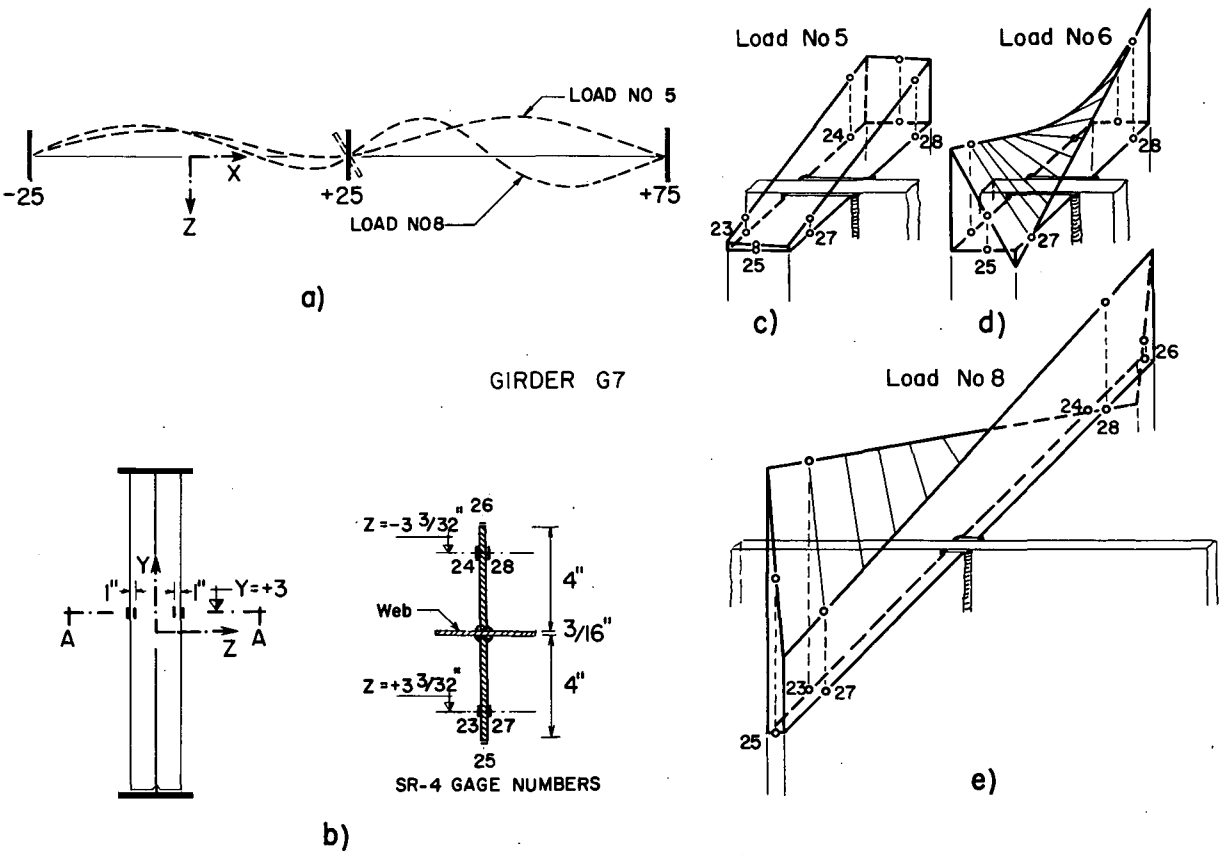


Fig. 3.23 Strain Measurements on a Transverse Stiffener.

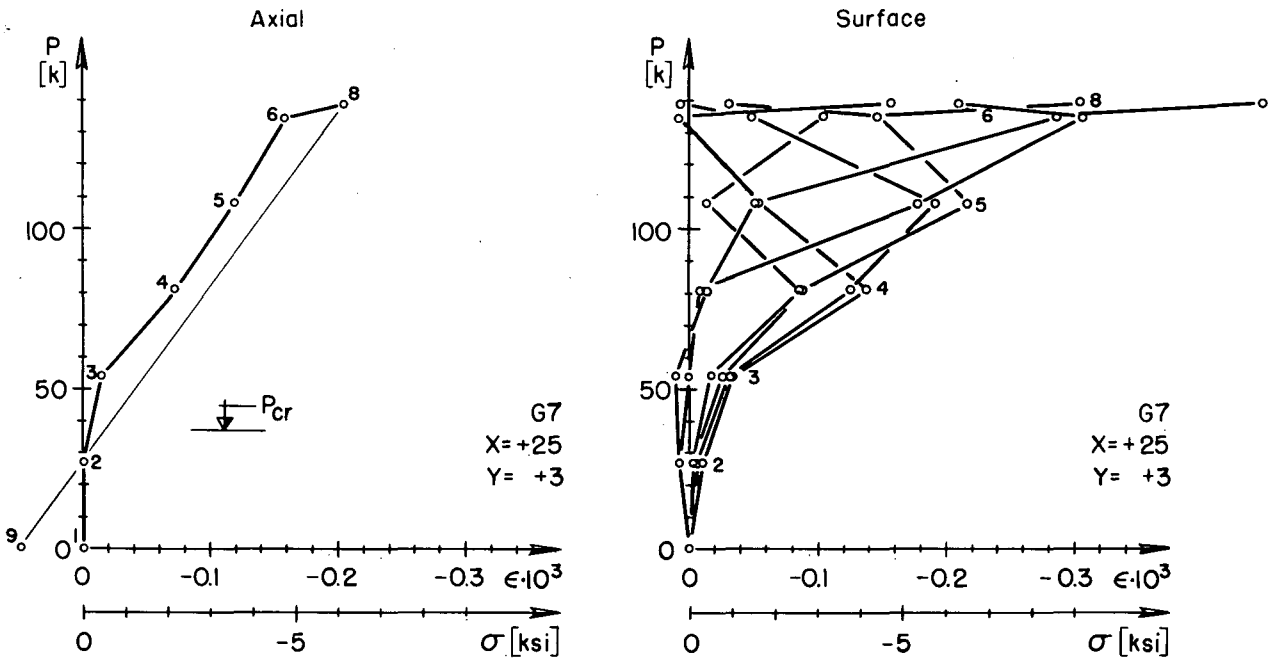


Fig. 3.24 Surface and Axial Stresses of a Transverse Stiffener, Girder G7

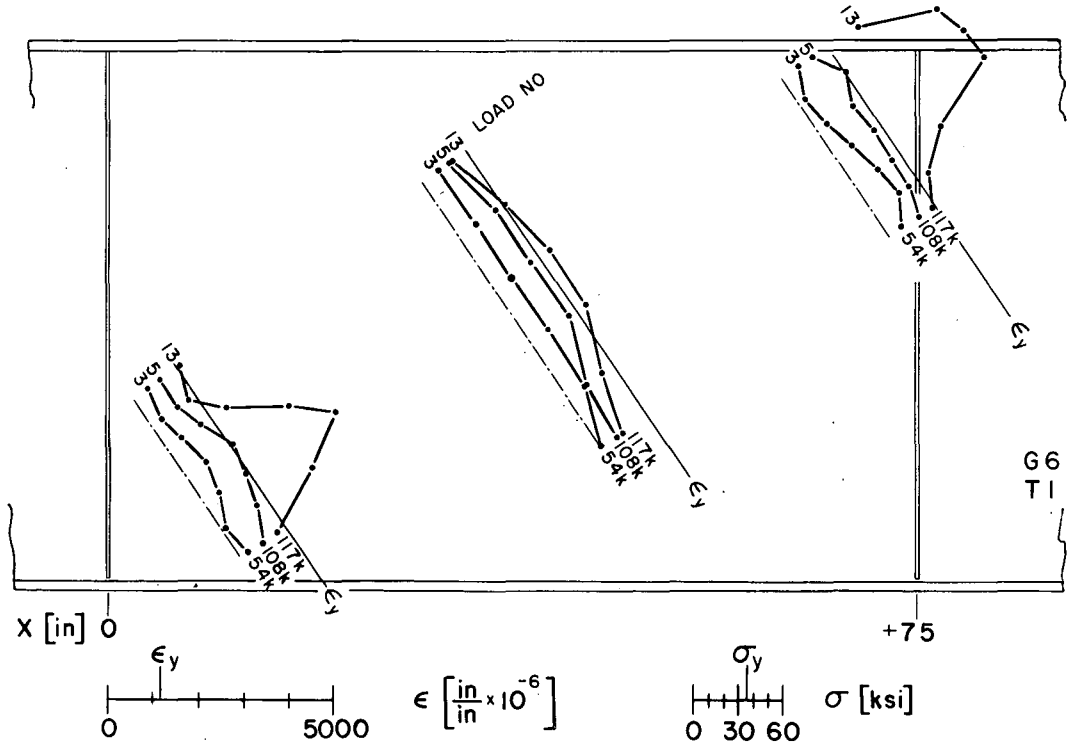


Fig. 3.25 Web Strains Determined by Whittemore Gage, Girder G6

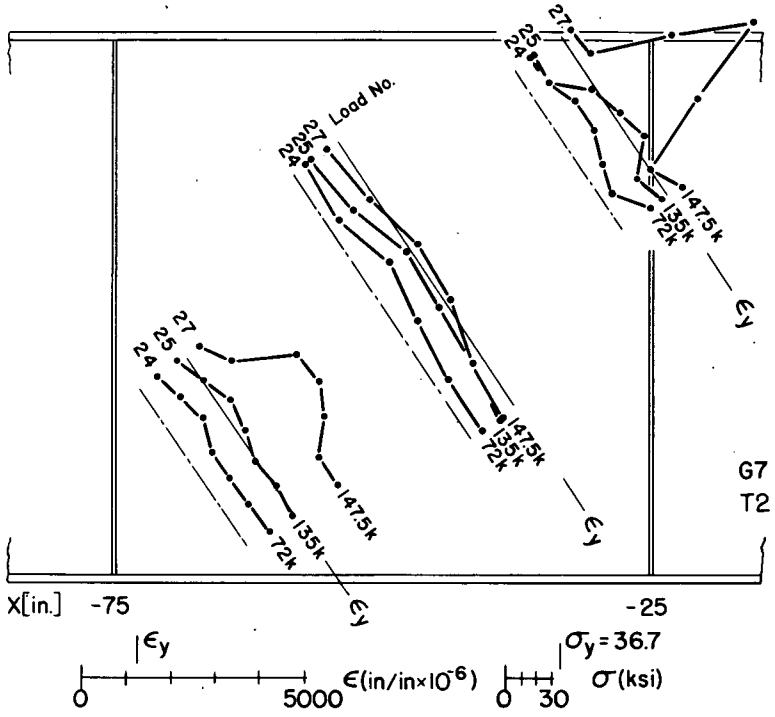


Fig. 3.26 Web Strains Determined by Whittemore Gage, Girder G7

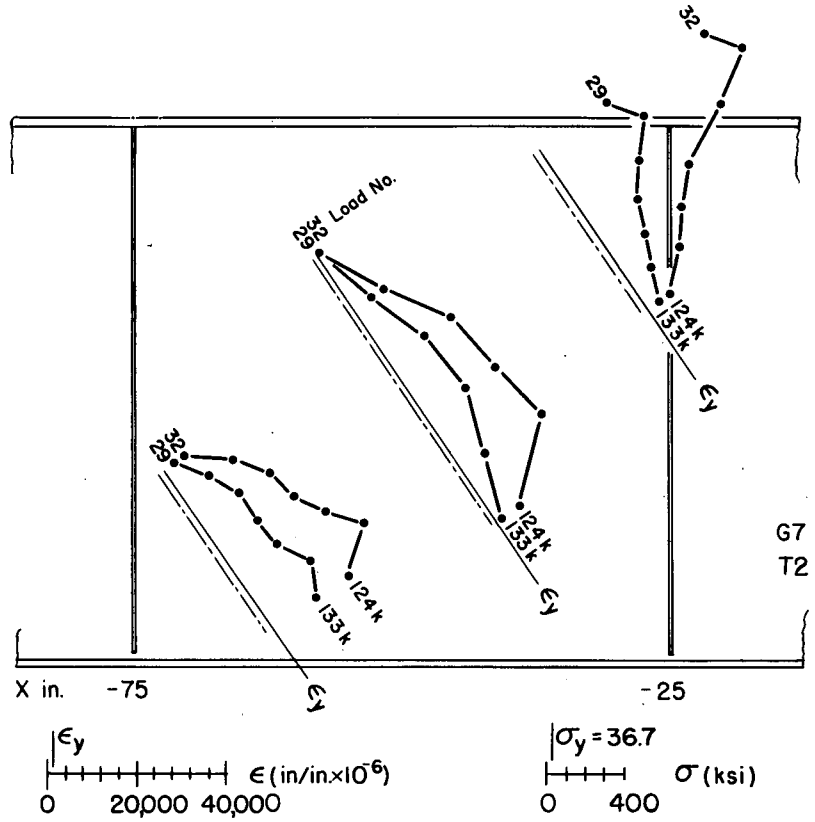


Fig. 3.27 Web Strains Determined by Whittemore Gage, Girder G7

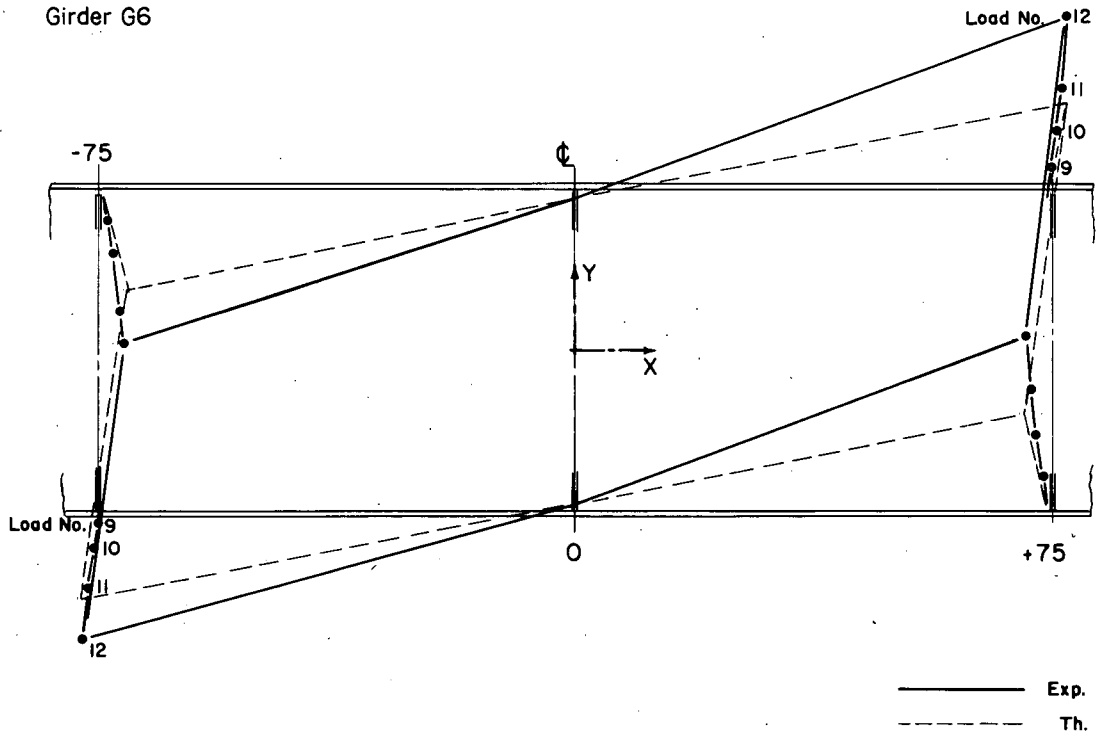


Fig. 3.28 Panel Deformation, Girder G6

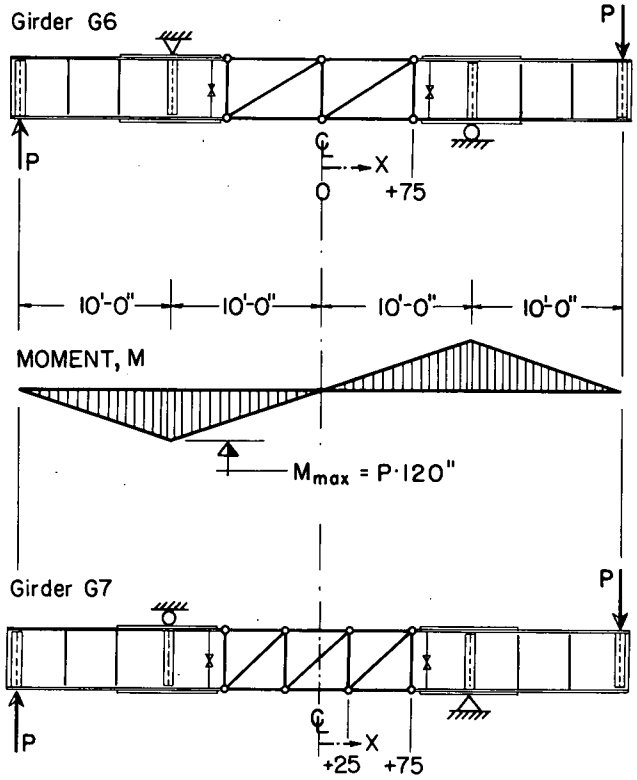


Fig. 3.29 Fictitious Trusses